1. INTRODUCTION

1.1 Historical background

The Merensky, UG2 and Plat Reefs of the Bushveld Complex contain about 75% and 50%, respectively, of the world's reserves of platinum and palladium (Cawthorn, 1999). However, for many years the UG2 layer remained unexploited, mainly due to seemingly insurmountable problems associated with its beneficiation. The gravity separation processes, used to upgrade the Merensky ore, proved to be unsuitable for the UG2 ore with its smaller PGE mineral grain sizes. Later, when flotation processes were considered, the need to maintain chromite recovery below the critical level determined by the smelting process, and yet maximise PGE recoveries, presented a new set of problems (Corrans *et al.*, 1982; Overbeek *et al.*, 1985; Hiemstra, 1988b; Hossy, 1991).

Since exploitation of the UG2 ore would have more than doubled resources, the incentive for development of a suitable process was high. In addition, the higher rhodium content of the UG2 ore, the production of chromite as a potentially valuable by-product, the higher PGE+Au content at some localities, and the fact that it could be mined using existing facilities, were further advantages (Brugman, 1985; Overbeek *et al.*, 1985; *Anon.*, 1987; Hossy, 1991).

After extensive research and testwork at Mintek and Western Platinum Mine, the metallurgical extraction problems were largely overcome (Corrans *et al.*, 1982; Overbeek *et al.*, 1985; Liddell *et al.*, 1986; *Anon.*, 1988; Hossy, 1991). The first plant to treat UG2 ore on its own was commissioned at Western Platinum Mine in 1984 (Brugman, 1985).

Typically, concentrate containing ~300 to 400 g/t PGE+Au and ~3% Cr_2O_3 (Vermaak, 1995) is produced from UG2 ore by means of multistage size reduction and froth flotation. This concentrate is subjected to matte smelting, followed by a converting step. The next step is the separation of the base metals from the precious metals by hydrometallurgical treatment of the matte, or by magnetic separation of PGE-rich Cu-Ni±Fe alloy after slow cooling. The final phase is the refining step, which involves the separation and purification of the six PGEs, gold and silver.

1.2 Reasons for undertaking this study

Mineralogical analysis provides information that can be used to predict and explain the behaviour of ores, minerals, and metallurgical products in metallurgical processes. The mineralogical characterisation of a suite of samples, consisting of unbroken ore, as well as samples generated during comminution and concentration, leads to a better understanding of the mineralogical factors affecting the behaviour of an ore during extraction. Additional improvements in recovery can be attained if the questions of where and why losses occur can be answered with some degree of confidence.

Flotation processes are being fine-tuned to allow for the beneficiation of more and more complex ores. Flow sheets are becoming more complicated with flotation conditions geared towards very specific types of particles (Koniggsman, 1985; Wesely, 1985; Kallioinen & Heiskanen, 1993). This is only possible with the aid of reliable mineralogical information.

Total PGE+Au recoveries to the flotation concentrates of UG2 ore are generally between 80 and 90 per cent, which means that significant amounts of valuable metals are lost to the flotation tailings. Much of these losses can be attributed to mineralogical factors. Large lateral variations exist in the characteristics of the UG2 layer. These differences pertain to the thickness of the layer (McLaren, 1980; McLaren & DeVilliers, 1982; Gain, 1985; 1986; Mossom, 1986; Von Gruenewaldt *et al.*, 1990; Davey, 1992; Maier & Eales, 1994; Lea, 1996; Maier & Bowen, 1996), chromite composition (McLaren, 1980; McLaren & DeVilliers, 1982), the vertical distribution of the PGEs (McLaren, 1980; McLaren & DeVilliers, 1982; Gain, 1985; Hiemstra, 1985, 1986; Mossom, 1986; Viljoen *et al.*, 1986a, b; Von Gruenewaldt *et al.*, 1990; Grimbeek, 1995), the grade and relative proportions of PGEs (McLaren & DeVilliers, 1982; Gain, 1985; Edwards, 1988; Viljoen & Schürmann, 1998) and the mineralogy, particularly of the base-metal sulphides and PGE minerals (McLaren, 1980; McLaren & DeVilliers, 1982; Kinloch, 1982; Peyerl, 1982; Von Gruenewaldt *et al.*, 1990; Winkels-Herding *et al.*, 1991; Hofmeyr & Adair, 1993; Grimbeek, 1995). However, the effect of variations in mineralogical parameters on the behaviour of UG2 ore during processing is still poorly understood.

There are several reasons for this:

- The major players in the platinum industry in South Africa (Anglo Platinum and Impala Platinum) have traditionally concentrated more on exploitation of the Merensky Reef. This situation has been changing over the past few years (Vermaak, 1995).

- In addition, the atmosphere of secrecy prevailing in the platinum industry means that even where research is being done on this subject, the results are generally not published.

- The mineralogy of UG2 ore and metallurgical product samples is difficult to characterise. PGE grades are low - ±5 g/t and <1 g/t for flotation feed and tailings samples respectively. In addition, the PGEs in the UG2 chromitite occur both as discrete, microscopically visible, PGE mineral grains (McLaren & de Villiers, 1982; Peyerl, 1982; Hofmeyr & Adair, 1993; Winkels-Herding *et al.*, 1991; Grimbeek, 1995), and, to a lesser extent, sub-microscopically* in other phases, predominantly the base-metal sulphides (Paktunc *et al.*, 1990), and possibly also oxide and silicate minerals (Peyerl, 1983; Hofmeyr, 1998).

- For many years the electron microprobe (EMP) was the only technique available to quantitatively determine the distribution of trace quantities of PGEs occurring sub-microscopically in other minerals, in particular the base-metal sulphides. The minimum detection limits achievable using EMP are relatively high (a few hundred ppm) (Cabri, 1991) making it impossible to calculate satisfactory PGE mineralogical mass balances for this type of deposit. Over the past twenty years major advances have been made in this field. Recently, detection limits as low as 10 ppm have been reported using improved electron-microprobe techniques (Johanson & Kojonen, 1995; Weiser *et al.*, 1998). Detection limits of a few ppm

---

* Cabri (1992) defines sub-microscopic PGE as PGE occurring as finely divided 'invisible' mineral grains less than 0.1μm in diameter, colloidal-size particulates, clusters of less than ~ 100 atoms, or true solid solution.

can be achieved with the proton microprobe using PIXE (Particle Induced X-Ray Emission) (Cabri *et al.*, 1984, Paktunc *et al.*, 1990; Cabri, 1992, Czamanske *et al.*, 1992), and down to the ppb range using SIMS (Secondary Ion Mass Spectrometry) (Ripley & Chryssoulis, 1994; Cabri & McMahon, 1995; 1996; Oberthür *et al.*, 1997).

Despite these developments only one set of measurements of PGEs in the base-metal sulphides of the UG2 chromitite has been published (Paktunc *et al.*, 1990). There are several reasons for this – for one thing, such instruments are not readily available, nor are suitable calibration standards. For another, in the UG2 chromitite, the base-metal sulphides themselves occur in trace amounts and as small grains.

- Very little attention has been given to techniques to characterise the mineralogy of the microscopically visible PGE minerals. In addition to being present in trace amounts, the PGE minerals are usually so fine-grained, and so difficult to identify, that traditional mineralogical techniques such as ore microscopy and X-ray diffraction provide insufficient information (Hiemstra, 1988a).

SEM-based image analysis techniques have been successfully applied in a variety of mineral processing related problems (Miller *et al.*, 1982; Petruk, 1983; 1988b; Dilks & Graham, 1985; Petruk & Smith, 1989; Gottlieb *et al.*, 1993; Van den Heever, 1995; Lastra *et al.*, 1999, to name but a few). Automated image analysis allows for the collection of statistically valid data in a reasonable time. In many cases, the image analyser makes it possible to carry out measurements on a scale which was out of the question using manual means, even though it was theoretically possible. However, the use of such techniques for the characterisation of PGE-bearing ores, remains a largely untested option. This aspect formed the focus of the present study.

1.3 Previous work

McLaren (1980) and McLaren and de Villiers (1982) reported on a mineralogical study of UG2 ore from different localities. Data on more than 6000 individual PGE mineral grains were collected manually, providing the first quantitative evaluation of

the PGE mineralogy of the UG2 chromitite layer. McLaren concluded that the mineralogy of UG2 chromitite varies from one location to the next, giving rise to different PGE+Au recoveries. Data collected by other researchers (Kinloch, 1982; Peyerl, 1982; Winkels-Herding *et al.*, 1991; Hofmeyr & Adair, 1993; Grimbeek, 1995) also indicated variations in the mineralogical characteristics of UG2 chromitite, often related to geological disturbances such as pothole structures or ultrabasic pipes. Although most of these researchers did not dwell on the metallurgical implications of these variations, Hofmeyr and Adair (1993), investigating the changes in the mineralogy of the Merensky and UG2 reefs in areas affected by iron-rich ultrabasic pegmatoid replacement, reported lower than expected PGE+Au recoveries from such localities.

Peyerl (1983, 1992) found a definite relationship between the mode of occurrence of PGE minerals and PGE recovery. As the percentage of PGE minerals entirely enclosed in silicate and chromite increases, the PGE recovery decreases.

The work performed by these investigators highlights the need for reliable mineralogical techniques for the characterisation of the PGE mineralogy of the UG2 ore. The advent of increasingly faster and powerful image analysis systems now provides the opportunity to launch such studies.

1.5 Objectives

The objectives of this study were:

- To develop and explore the use of automated image analysis to characterise the mineralogy of UG2 chromitite ore and mineral processing products
- To determine how differences in the geological environment affect the mineralogy of the UG2 chromitite
- To determine whether variations in the mineralogy of the UG2 chromitite can be related to differences in flotation behaviour
- To identify the factors affecting the recovery of PGE mineral-bearing particles from UG2 chromitite.

2. GEOLOGY AND REGIONAL SETTING

2.1 General

The Bushveld Complex is one of the world's greatest geological phenomena. It is not only the largest known intrusion of its kind in the world, but also contains vast reserves of PGEs, chromium and vanadium, nickel, cobalt, copper, tin, iron, fluorspar, andalusite, magnesite and chrysotile asbestos (Willemse, 1964; Coetzee, 1976; Vermaak & Von Gruenewaldt, 1986).

Situated in the northern half of the Kaapvaal craton, the Bushveld Complex covers an area of approximately 65 000 km^2 (SACS, 1980) (Figure 1). The magmatic events resulting in the formation of the Bushveld Complex (2.05 to 2.06 Ga), commenced with the extrusion of the basic and acid volcanics of the Rooiberg Group along a regional unconformity, marking the top of the Transvaal sedimentary succession. Contemporaneous with the Rooiberg volcanism, the Rashoop Suite granophyre was emplaced. This was followed by the emplacement of the layered ultrabasic to basic intrusives of the Rustenburg Layered Suite, and subsequently the intrusion of the Bushveld Granites (Lebowa Granite Suite) (Cheney & Twist, 1988; Walraven *et al.*, 1990; Walraven & Hattingh, 1993; Schweitzer *et al.*,1995; Schweitzer & Hatton,1995a; 1995b; Walraven, 1997).

2.2 The Rustenburg Layered Suite

The Rustenburg Layered Suite comprises a 7000-9000 m thick pile of basic and ultrabasic rocks which is informally subdivided into five zones, namely the Upper, Main, Critical, Lower and Marginal Zones (Figure 2) (SACS, 1980; Walraven, 1986; Von Gruenewaldt *et al.*, 1985). The UG2 chromitite forms part of a series of chromitite layers, traditionally divided into the Lower Group, Middle Group and Upper Group chromitites, present in the Critical Zone (Cousins & Feringa, 1964; Von Gruenewaldt *et al.*, 1986; Vermaak, 1995).

The Lower Group chromitites (numbered LG1 to LG7 from the bottom upwards) occur within the pyroxenites of the lower part of the Critical zone. The Middlle Group chromitites (MG1 to MG4) straddle the boundary between the pyroxenitic lower and plagioclase-rich upper part of the Critical Zone. The Upper Group

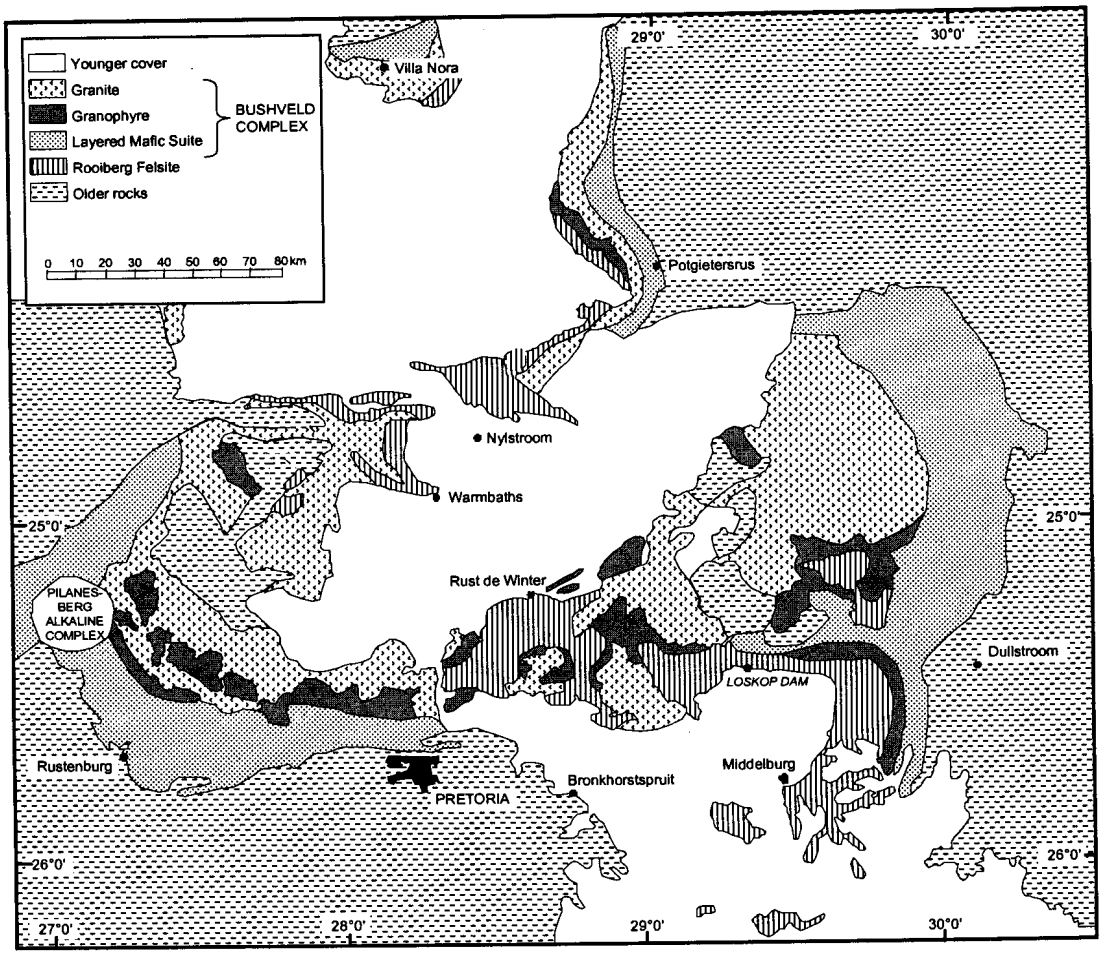

Figure 1 *Geological sketchmap showing the distribution of the rocks of the Bushveld Complex. (Courtesy of Department of Earth Sciences, University of Pretoria)*

chromitites, UG1 and UG2 (indicated in Figure 2), are found near the top of the Critical Zone. The Upper Critical subzone also hosts the platiniferous Merensky Reef.

2.3 The UG2 chromitite layer

The UG2 layer is located near the base of a 5 to 12 m thick felspathic pyroxenite layer, situated in the succession between the UG1 chromitite layer below, and the Merensky Reef above (Figure 2). Except for a few local interruptions, it can be followed continuously along strike in both the eastern and western portions of the Bushveld Complex (McLaren & de Villiers, 1982; Davey, 1992; Maier & Eales, 1994; Maier & Bowen, 1996).

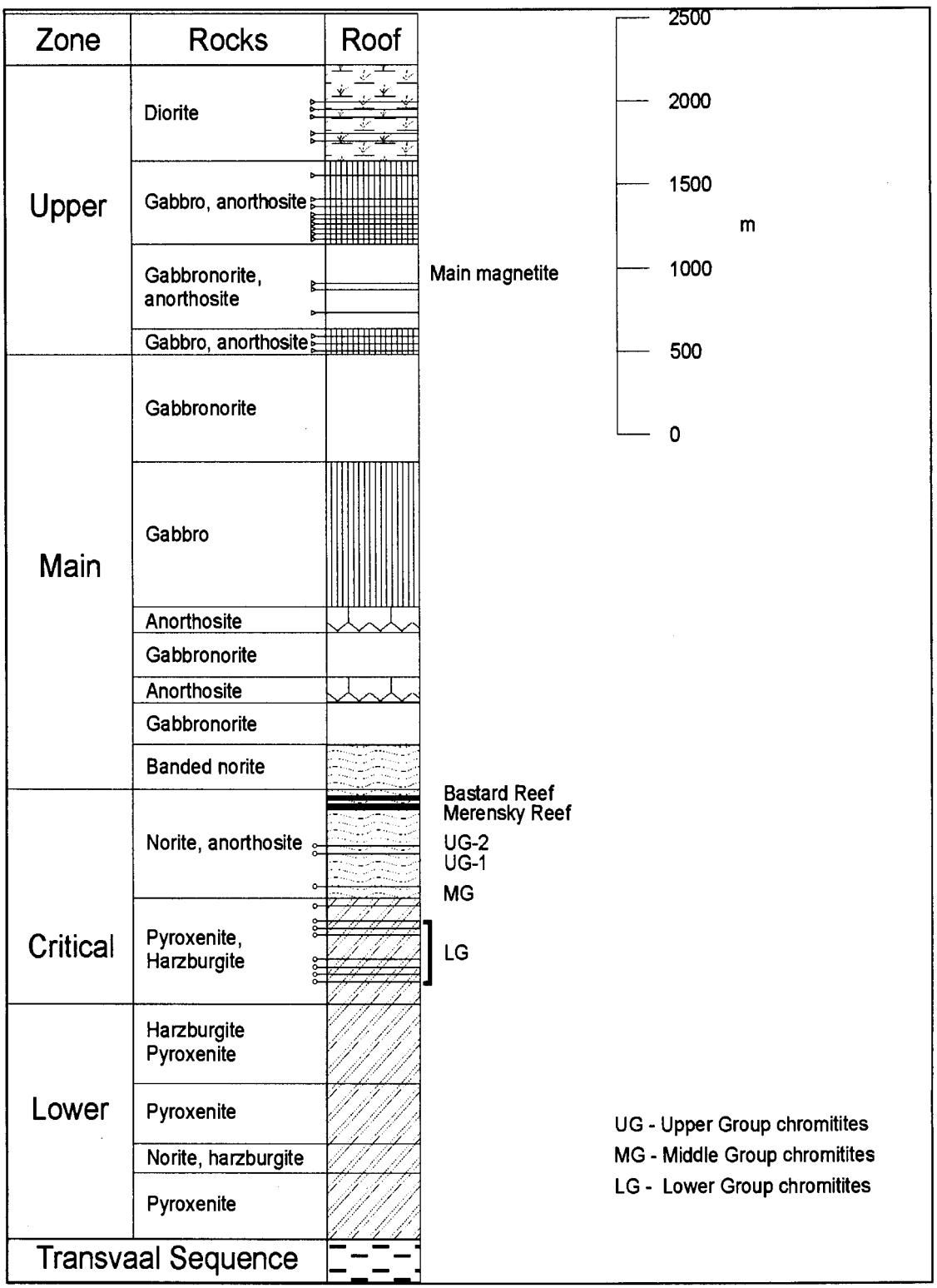

Figure 2 *Stratigraphic succession of the Rustenburg Layered Suite (after Vermaak, 1995). Chromitite and magnetite layers are indicated by o— and >— respectively.*

The thickness of the UG2 chromitite layer is usually about 1 m. A variable number of thin leaders (10-15 cm) may be present within the overlying UG2 pyroxenite, up to 3 m above the main layer (McLaren, 1980; McLaren & de Villiers, 1982; Gain,1985; 1986; Mossom, 1986; Davey, 1992; Maier & Eales, 1994; Lea, 1996; Maier & Bowen, 1996).

The UG2 layer has in many places been disrupted by late- to postmagmatic structures such as faults, potholes and iron-rich ultrabasic replacement pegmatoids. As will be discussed below, much of the reported mineralogical variation in the UG2 chromitite can be related to such disturbances. The following 'types' of UG2 chromitite have been described:

2.3.1 Undisturbed or normal UG2

In many areas the UG2 chromitite appears to be relatively undisturbed with few signs of replacement, cataclasis, recrystallisation, or talcification, with a footwall of either norite or anorthosite (Farquhar, 1986; Hiemstra, 1986; Davey,1992; Maier & Bowen, 1996; Van der Merwe *et al.*, 1998). Normal UG2 chromitite consists predominantly of chromite (60-90 volume per cent) with interstitial orthopyroxene and plagioclase. Chalcopyrite, pyrrhotite, pyrite and pentlandite are the major base-metal sulphide minerals, usually present in trace amounts at chromite-silicate grain boundaries. The PGE minerals are predominantly sulphides, mostly laurite, cooperite, an unnamed Pt-Rh-Cu-Ir-sulphide, braggite, an unnamed Pt-Pb-Cu-sulphide, and rarely, vysotskite. These minerals tend to be strongly associated with base-metal sulphide minerals, exhibiting a preference to occur at grain boundaries of base-metal sulphides with chromite and/or silicate (McLaren, 1980; McLaren & de Villiers, 1982; Viljoen & Hieber, 1986; Viljoen *et al.*, 1986a; Hiemstra, 1988b; Grimbeek, 1995).

2.3.2 UG2 with pegmatoid footwall

The UG2 chromitite is in many places underlain by a coarse-grained felspathic pegmatoid (Viljoen *et al.*, 1986b; Hiemstra, 1988a; Cawthorn & Barry, 1992; Davey, 1992; Van der Merwe *et al.*, 1998). Cawthorn and Barry (1992) reported that this pegmatoid has essentially the same mineralogy and texture as underlying pyroxenites, only the grain size is coarser. These authors postulated that the introduction of hot

primitive magma caused recrystallisation of pyroxenite, producing the coarse grain size.

During recrystallisation of the footwall, some changes also occurred in the UG2 chromitite layer itself (Hiemstra, 1985). In places the chromitite foundered and slumped into the underlying pegmatoid. Hiemstra (1985) estimated that the UG2 layer could have lost a few centimetres in this manner. Sintering (annealing or densification) of chromite, a process during which the chromite grains are enlarged until they border against each other, eliminating interstitial silicates, may be linked to this type of recrystallisation (Hiemstra, 1985; Hiemstra, 1988a, b). Redistribution of copper and nickel, and to a lesser extent the PGEs, can occur (Hiemstra, 1985). Hiemstra (1988a) speculated that changes in the grain size of base-metal sulphides and PGE minerals may occur.

2.3.3 Iron-rich ultrabasic replacement pegmatoid

Iron-rich ultrabasic pegmatoid replaced the UG2 chromitite and its associated rocks in some places (Viljoen & Scoon, 1985; Gain, 1985; Leeb-du-Toit, 1986; Viljoen *et al.*, 1986a, b; Viljoen & Hieber, 1986; Farquhar, 1986; Hofmeyr & Adair, 1993; Grimbeek, 1995). These pegmatoids are often transgressive, and their chemical effects on the surrounding lithologies are extensive. The introduction of iron, titanium, vanadium and calcium (Viljoen *et al.*, 1986b; Grimbeek, 1995) causes the formation of phases such as titaniferous magnetite and ilmenite (Viljoen & Scoon, 1985; Hiemstra, 1988b; McLaren & De Villiers, 1982; Grimbeek, 1995).

An increase in the grain sizes of chromite, sulphides, and possibly the PGE minerals, have been reported (Hiemstra, 1988b; McLaren & de Villiers, 1982; Grimbeek, 1995). Alteration of orthopyroxene and plagioclase results in the formation of low temperature hydrous silicates such as amphibole, chlorite, talc, serpentine and clay minerals (Grimbeek, 1995). The magmatic sulphides may be replaced by low temperature sulphides such as millerite, violarite, heazlewoodite, chalcocite, covellite and bornite (Hiemstra, 1988b; Grimbeek, 1995). In other places, the appearance of coarse sulphide blebs (up to 2 mm in diameter), rich in pyrrhotite, was noted (Hiemstra, 1988a; Hiemstra, 1988b; Grimbeek, 1995). Hiemstra (1988b) also reported the replacement of pyrrhotite by magnetite in some samples.

The PGE mineral assemblage is dominated by non-sulphide minerals such as alloys of Pt, Pd and Rh with Cu and Fe, PGE sulpharsenides, and Pt and Pd compounds with Sb, Bi, Te, Hg and Pb (Hiemstra, 1988b; Hofmeyr & Adair, 1993; Grimbeek, 1995).

2.3.4 UG2 associated with pothole structures

In plan, potholes are roughly circular structures, disturbing the UG2 and its surrounding lithology, causing the UG2 chromitite to occur below its normal stratigraphic elevation. They may be up to several hundred metres wide, and range from a few metres to several tens of metres deep, varying from gentle slump structures, in which the UG2 is continuous but transgresses the footwall units (Figure 3), to carrot-shaped structures in which the UG2 is broken up. Pothole structures have been reported from all over the Bushveld Complex (Leeb-Du Toit, 1986; Viljoen *et al.*, 1986a, b; Viljoen & Hieber, 1986; Farquhar, 1986; Mossom, 1986; Gain, 1986; Cawthorn & Barry, 1992; Hahn & Ovendale, 1994; Lea, 1996; Van der Merwe *et al.*, 1998; Lomberg *et al.*, 1999).

In the case of the Merensky Reef, pothole formation is associated with changes in mineralogy and mineral chemistry in the vicinity of these structures. Pegmatoidal textures, increased replacement of magmatic silicates by low temperature hydrous phyllosilicates, the presence of graphite, changes in chromite composition, and the appearance of Pt-Fe alloys as a major component of the PGE mineral assemblage have been reported (Buntin *et al.*, 1985; Ballhaus, 1988; Kinloch & Peyerl, 1990; Reid *et al.*, 1993).

Theories concerning the origin of these features abound. These theories include mechanical scouring (Schmidt, 1952), thermochemical erosion (Campbell, 1986), and the upward movement of residual magmatic liquids and/or hydrothermal fluids (Buntin, *et al.*, 1985; Ballhaus, 1988; Cawthorn & Poulton, 1988; Boudreau, 1992; Reid *et al.*, 1993). The possibility of a genetic relationship between Fe-rich replacement pegmatoid and potholes has been suggested by several investigators (Viljoen & Hieber, 1986; Farquhar, 1986; Kinloch & Peyerl, 1990).

While the involvement of a fluid phase would explain the observed changes in mineralogy, isotopic evidence presented by Carr *et al.* (1999), indicated that there was no interaction between footwall material and the overlying magma during, or after, the

formation of Merensky Reef potholes. These authors postulated that potholes represent structural features formed during depocenter subsidence (Carr *et al.*, 1994a, b), with laterally migrating Merensky magma providing the fill-in material (Carr *et al.*, 1999), offering no explanation for the reported changes in mineralogy.

No published information is available on the mineralogy of the UG2 layer in the vicinity of pothole structures. Cawthorn and Poulton (1988), during a study of pegmatoid underlying the UG2 chromitite, found no evidence of the involvement of a fluid phase during the formation of UG2 potholes.

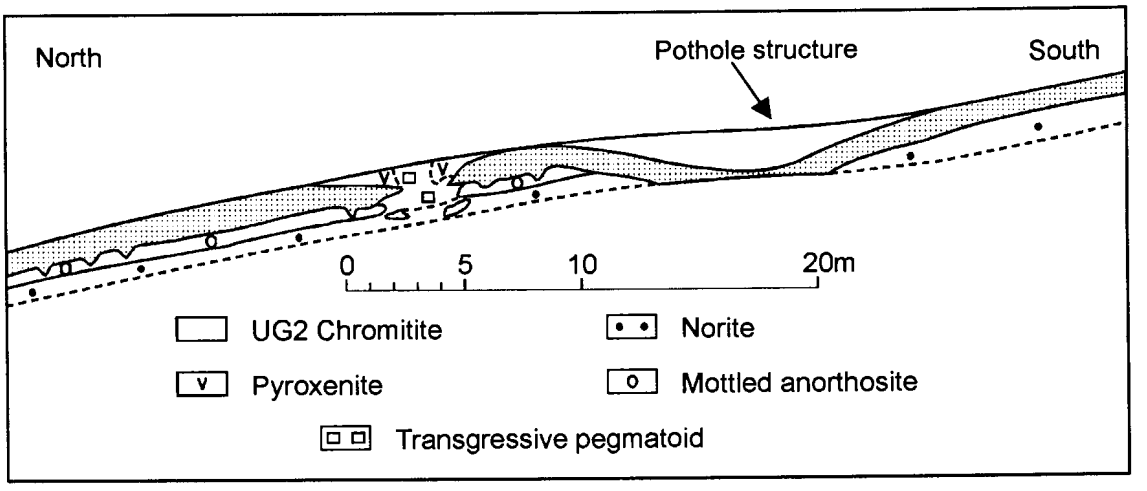

Figure 3 *Cross section through a pothole structure in the UG2 ore (Farquhar, 1986).*

2.3.5 Faulted and fractured UG2 chromitite

The rocks of the Bushveld Complex have commonly been disrupted by faulting and fracturing (Gain, 1986; Viljoen & Hieber, 1986; Viljoen *et al.*, 1986a, b). Cataclastic textures, as well as an increase in the concentration of hydrous phyllosilicate phases, can be observed in the UG2 chromitite in faulted areas (Hiemstra, 1988a).

The formation of massive chromitite from faulted areas have been reported by Kupferbürger *et al.* (1937). Worst (1986) contends that the formation of this type of ore appears to be a very localised feature, becoming friable within centimetres into surrounding unfractured ore.

Late stage fracturing, creating pathways along which fluids migrated, is widespread. Some redistribution of sulphides and PGE minerals may be found along these cracks (Hiemstra, 1988a). Schiffries and Skinner (1987) reported extensive alteration of the silicate minerals in the wallrock adjacent to fractures.

2.3.6 UG2 chromitite exposed to surface weathering

Another important alteration process, known to affect recovery processes, is surface weathering. During sample collection, sampling of weathered material was studiously avoided, as the effects of supergene alteration are beyond the scope of this investigation.

3. SAMPLING STRATEGY

3.1 Project outline

To achieve the stated objectives, the mineralogy, chemistry and flotation behaviour of fourteen samples of UG2 ore were compared as outlined in Figure 4. Each sample was crushed to <2 mm to produce a sample with mineralogical and chemical characteristics representative of unbroken ore. This was followed by comminution and rate flotation tests on each sample. Mineralogical and chemical analysis were performed on samples of crushed ore, milled feed and flotation products.

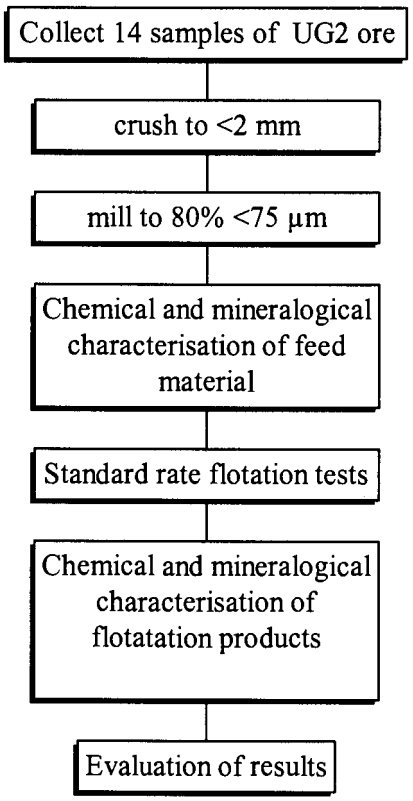

Figure 4 *Outline of experimental treatment of fourteen samples of UG2 ore.*

3.2 Sample collection

Samples were collected underground on the Lonrho mining property in the Marikana-Brits area (Figure 5). Appropriate sampling locations were identified and described by Lonrho geologists to include a variety of different "types" of UG2 chromitite. The rationale behind the sampling scheme was to obtain samples of UG2 ore with as wide a variation in mineralogical characteristics, and consequently flotation behaviour, as possible.

For reasons of confidentiality, exact sample locations cannot be disclosed. Fourteen samples were taken from three different mining areas (denoted A, B and C). A description of the geological context of each sample is given in Table 3.1. Note that Area C is characterised by more disruptions such as faults, potholes and dolerite dykes, compared to Areas A and B.

Sampling was complicated by the fact that the UG2 chromitite at a specific location had frequently been subjected to a combination of different geological disturbances. For example, sample B3, taken at the edge of a pothole, may also have been affected by iron-rich ultrabasic replacement pegmatoid present in the vicinity.

Composite samples were obtained by cutting channels across the UG2 chromitite, including ±1 cm of footwall and hangingwall respectively. In order to make up enough mass for flotation tests on each sample, a number of channels were cut adjacent to one another. The composite samples were despatched to Mintek in sample bags, where further observations on the macroscopic appearance of the samples were made by the investigator. With the exception of sample A5, all of the samples were relatively friable, crumbling upon being handled.

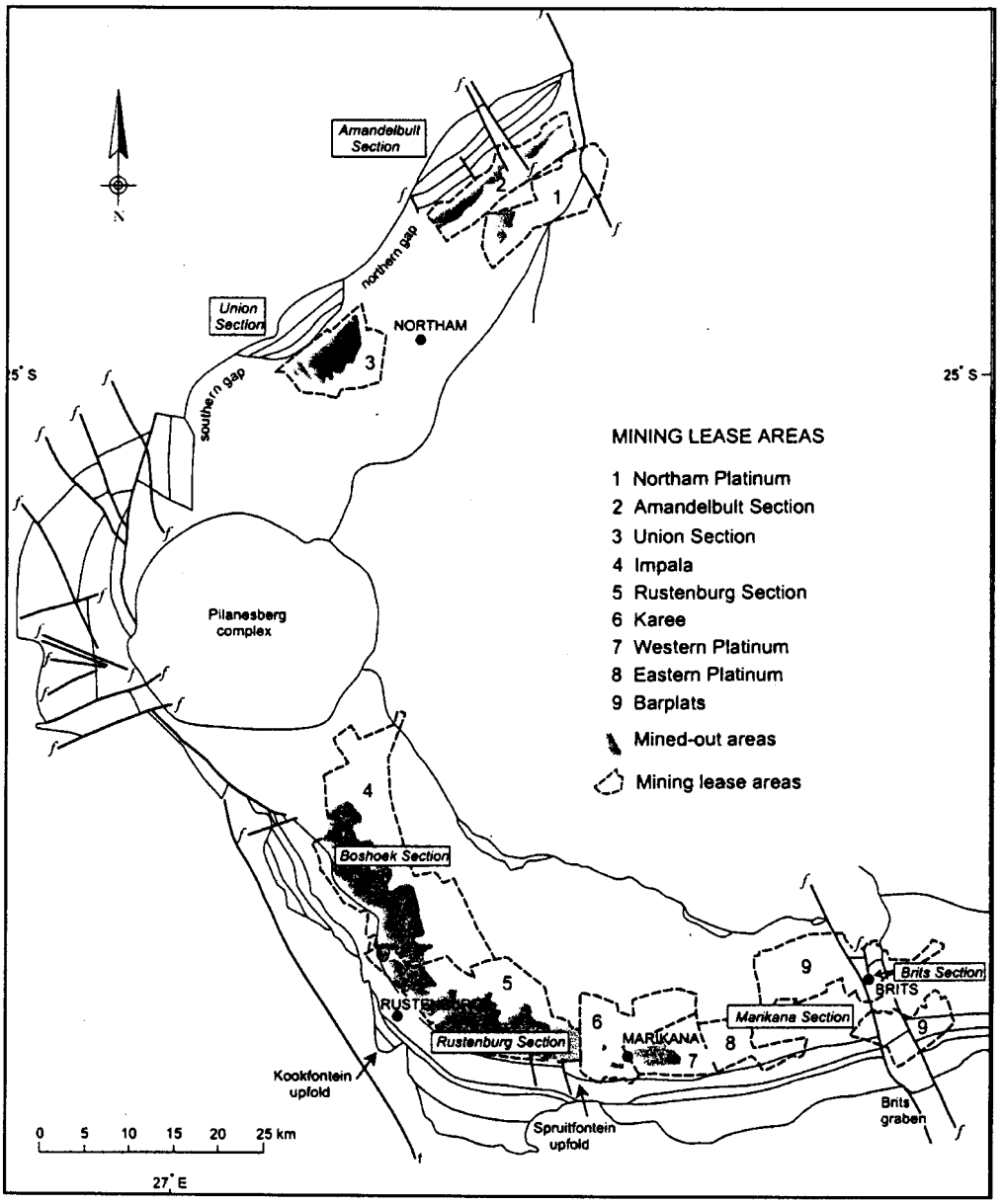

Figure 5 *Lease boundaries of the main platinum-mining operations in the Western Bushveld Complex (after Viljoen & Schürmann, 1998).*

Table 3.1 Sample description

Sample	Origin	Comments
A2	UG2 chromitite with mottled anorthosite footwall.	Lenses of coarse sugary chromite common.
B2	UG2 chromitite with norite footwall.	
A1	UG2 chromitite with pegmatoid footwall.	Anorthositic lenses with phlogopite.
B1	UG2 chromitite with pegmatoid footwall. Iron-rich ultrabasic replacement pegmatoid in the vicinity.	Extremely friable
A3	UG2 chromitite with pegmatoid footwall on the downdip side of a pothole structure.	
B3	UG2 chromitite with pegmatoid footwall taken at the edge of a pothole. Iron-rich ultrabasic replacement pegmatoid in the vicinity.	Sintering of chromite grains visible in places. Friable and coarse-grained.
A4	UG2 chromitite with footwall consisting of iron-rich ultrabasic replacement pegmatoid.	Sintering of chromite grains could be seen at the bottom of the layer. In places quite coarse-grained and crumbly. Lenses and bands of anorthosite (±0.5 cm thick).
B4	UG2 chromitite with pegmatoid footwall taken next to a fault. Iron-rich ultrabasic replacement pegmatoid footwall in the vicinity.	Pitch black and coarse-grained with high degree of sintering of chromite grains. Associated with pegmatitic veins consisting of quartz, hornblende and biotite.
A5	UG2 chromitite in fault zone. Iron-rich ultrabasic replacement pegmatoid in the vicinity.	The general appearance of the sample is extremely fine-grained and massive. Abundant veins of secondary minerals.

Table 3.1 continued *Sample description.*

Sample	Location	Comments
C1	UG2 chromitite at the edge of a pothole structure.	Coarse calcite veins present. Abundant hydrous silicates along shear planes and in veins. Sintering of chromite grains in places. Coarse and crumbly.
C2	UG2 chromitite in an area where the pegmatoid footwall pinches out. The footwall consists of a 2 cm thick anorthosite band followed by norite.	Relatively hard sample, even where coarse-grained. The hardest sample from area C.
C3	UG2 chromitite from a fault zone.	Criss-crossed by veins of hydrous silicates and quartz. Relatively hard and cohesive.
C4	UG2 chromitite with pegmatoid footwall. About 50 m from the pothole in C1.	Relatively hard. Occasional cracks healed by secondary minerals such as hydrous silicates.
C5	This sample was taken from an area where the UG2 chromitite layer is characterised by the presence of an anorthosite band, sharp top and bottom, approximately 6 cm thick. About 20 m from a dolerite dyke.	Relatively hard. Similar to C2 and C4. Very little signs of alteration. No veins visible.

4. METHOD

4.1 Comminution

Liberation of the valuable components of an ore, in this case PGE minerals and base-metal sulphides, from the gangue minerals is accomplished by comminution, i.e. crushing and milling, to such a degree that the product approaches a mixture of liberated particles of valuable minerals and gangue.

For the purpose of this project, each sample was subjected to jaw crushing followed by cone crushing to reduce the particle size to <2mm. A representative sub-sample of each sample at <2mm was taken for mineralogical and chemical analysis. A rotary sample splitter was used to ensure that sub-samples were obtained in a representative manner.

The remainder of the sample was crushed to <1.7 mm before milling to 80% <75 μm in a rod mill, using standard milling procedures for this type of ore.

4.2 Froth flotation

4.2.1 ***General principles*** (Gaudin, 1957; Rogers, 1962; Wills, 1981; Herrera-Urbina *et al.*, 1990)

Froth flotation involves the chemical treatment of a mixture of ground ore and water to create conditions favourable for the attachment of certain mineral particles to air bubbles. The air bubbles carry the selected minerals to the surface of the pulp and form a stabilised froth, which is skimmed off, while the other minerals remain submerged in the pulp.

Whether or not a mineral can be recovered by flotation, is determined by its surface characteristics. A surface formed by rupture of Van der Waals bonds does not readily attach to water dipoles, and will be hydrophobic (water-repellant). Minerals characterised by this type of surface are naturally floatable and include graphite, sulphur, molybdenite and talc.

In contrast to this, a surface formed by the rupture of covalent or ionic bonds can chemically react with the environment and is therefore hydrophylic. The surface

characteristics of minerals can be modified to create hydrophobic surfaces by the interaction with flotation reagents (collectors and activators). The xanthate collector used to promote flotation of the sulphide minerals will generally not attach to oxide and silicate gangue minerals. To further ensure that gangue minerals do not float, depressants, which enhance the hydrophylic nature of the gangue minerals, are added to the system.

4.2.2 Standard rate flotation tests

Since the purpose of the rate flotation tests were to determine the effect of changes in the mineralogy of the ore on the flotation behaviour, all other factors (equipment, operating factors and reagents) affecting flotation response were kept constant for all samples.

Conditions of rate flotation tests

Standardised rate flotation tests were carried out by the Minerals Processing Division at Mintek. A standard 3*l* Denver laboratory flotation cell was used for the flotation testwork. Froth was removed manually by operating two scraper blades simultaneously across the complete cell area every 15 seconds (Figure 6). The scraping depth was controlled at 0.6 cm below the overflow lip. Reagent conditions and contact times are listed in Table 4.1.

The ground ore was floated in one kilogram batches. Rougher concentrates were collected after 1, 3, 8, 15 and 20 minutes of flotation. Six kilograms of each sample had to be floated in this way to generate enough sample mass for chemical and mineralogical analysis.

After weighing of the wet concentrate and tailings fractions, excess water was filtered off, and solids dried in an oven. The dry samples were weighed and representative samples taken for chemical and mineralogical analysis.

Figure 6 *Operator performing rate flotation tests.*

Table 4.1 *Reagent additions and contact times*

Reagent dosage and contact times	*g/t*	*minutes*
*$CuSO_4.5H_2O$ (activator)**	40	5
SIBX (collector)	180	2
Norilose (depressant)	120	2
Dow 200 (frother)	30	1
Flotation	20 minutes	
pH	~9	
Temperature	~20 ° C	

* *The activator forms a precipitate on the surface of the sulphide minerals, thereby improving floatability and contact with the xanthate collector.*

Reproducibility of rate flotation tests

Reproducibility of rate flotation tests was determined from the mass recoveries obtained during flotation tests on eighteen 1 kilogram sub-samples of sample A1. The results reported in Table 4.2 show that the reproducibility of the rate flotation tests is acceptable with a relative error well below 10 per cent at the 95% confidence limit.

Interpretation of flotation test results

It has been demonstrated that plant rougher flotation results correlate better with differences in the rate of recovery in the laboratory, rather than with changes in equilibrium recovery (recovery at long flotation times) (Klimpel, 1980; 1988). Mathematical flotation models that incorporate both a recovery and a rate function can completely describe flotation time-recovery profiles and provide an excellent tool to evaluate flotation tests (Dowling *et al.*, 1985). Surprisingly small differences in rate flotation parameters in laboratory tests are real, and often much bigger, in a plant sense. Marais (1989) identified the modified Kelsall model (Kelsall, 1961) as being appropriate for the evaluation of the time-recovery profiles of PGE+Au from UG2 ore. This model is based on the assumption that PGE mineral-bearing particles have two distinct and different rates of flotation. The model states:

$$R = U\,[1-((1-\phi)\exp(-k_f t) + \phi \exp(-k_s t))]$$

where R = recovery at time t; ϕ = fraction of slow floating mineral; k_s = rate constant for slow floating mineral min^{-1}; k_f = rate constant for fast floating mineral min^{-1}; U = ultimate recovery at infinite time.

Application of this model to the PGE+Au data for sample A1 (Table 4.3 and Figure 7) indicates that the ultimate recovery, U, for PGE+Au in this sample, at a grind of 80%<75µm, and under the given flotation conditions, is 96 per cent. Of the floatable fraction, 18 per cent (∴ 16 per cent of the total PGE+Au) is slow-floating with a flotation rate constant of 0.22 min^{-1}, hence 96-16=80 per cent is fast-floating (flotation rate constant: 2.38 min^{-1}). Goodness of fit of the model was evaluated by a loss function, Loss=(Observed-Predicted)^2, i.e. the sum of the squared deviation about the predicted values. The better the fit, the closer to 0 the Loss value will be.

Table 4.2 *Mass recoveries to rougher concentrate after 1, 3, 8 15 and 20 minutes of flotation for eighteen 1 kilogram sub-samples of sample A1. Upper and lower confidence limits around the average were calculated for sets of six individual tests at the 95% confidence level using resampling statistics (Simon & Bruce, 1991).*

	Mass recovery (%)						**Cumulative mass recovery (%)**					
Flotation product	*RC1*	*RC2*	*RC3*	*RC4*	*RC5*	*RT*	*RC1*	*RC2*	*RC3*	*RC4*	*RC5*	*RT*
Time	*0-1 mins.*	*1- 3 mins.*	*3-8 mins.*	*8-15 mins.*	*15-20 mins.*		*0-1 mins.*	*1-3 mins.*	*3-8 mins.*	*8-15 mins.*	*15-20 mins.*	
Test #1	3.6	2.0	2.6	1.7	0.5	89.6	3.6	5.6	8.2	9.9	10.4	89.6
Test #2	3.8	2.3	2.6	1.5	0.5	89.4	3.8	6.0	8.6	10.1	10.6	89.4
Test #3	3.8	2.5	2.9	1.6	0.6	88.8	3.8	6.3	9.1	10.7	11.2	88.8
Test #4	4.1	2.5	2.7	1.6	0.5	88.6	4.1	6.5	9.3	10.9	11.4	88.6
Test #5	3.4	2.4	2.8	1.6	0.6	89.2	3.4	5.8	8.6	10.2	10.8	89.2
Test #6	3.3	2.5	2.8	1.7	0.5	89.2	3.3	5.8	8.6	10.3	10.8	89.2
Test #7	3.7	2.6	2.9	1.6	0.6	88.6	3.7	6.4	9.2	10.8	11.4	88.6
Test #8	4.0	2.4	2.7	1.5	0.7	88.8	4.0	6.4	9.1	10.6	11.2	88.8
Test #9	4.2	2.5	2.8	1.6	0.6	88.3	4.2	6.7	9.5	11.1	11.7	88.3
Test #10	4.3	2.9	3.0	1.5	0.5	87.8	4.3	7.2	10.2	11.7	12.2	87.8
Test #11	3.7	2.6	2.9	1.7	0.6	88.5	3.7	6.3	9.2	10.9	11.5	88.5
Test #12	3.2	2.4	2.8	1.5	0.6	89.5	3.2	5.6	8.5	9.9	10.5	89.5
Test #13	3.5	2.3	2.4	1.5	0.6	89.7	3.5	5.8	8.2	9.7	10.3	89.7
Test #14	4.1	2.2	2.8	1.6	0.6	88.7	4.1	6.3	9.1	10.8	11.3	88.7
Test #15	3.9	2.5	2.7	1.5	0.6	88.8	3.9	6.4	9.1	10.6	11.2	88.8
Test #16	3.4	2.1	2.5	1.5	0.6	89.9	3.4	5.5	8.0	9.5	10.1	89.9
Test #17	4.0	2.3	2.7	1.5	0.6	88.9	4.0	6.3	9.0	10.6	11.1	88.9
Test#18	3.6	2.2	2.3	1.4	0.6	90.0	3.6	5.8	8.0	9.4	10.0	90.0
Average	3.7	2.4	2.7	1.6	0.6	89.0	3.7	6.1	8.9	10.4	11.0	89.0
Lower limit	3.5	2.2	2.6	1.5	0.5	88.5	3.5	5.8	8.4	10.0	10.6	88.6
Upper limit	4.0	2.6	2.8	1.6	0.6	89.5	4.0	6.5	9.3	10.9	11.5	89.5
Absolute error %	0.3	0.2	0.1	0.1	0.1	0.5	0.3	0.4	0.5	0.5	0.5	0.5
Relative error %	6.7	8.3	3.7	3.2	8.7	0.6	6.7	5.7	5.1	4.3	4.1	0.5

RC = Rougher concentrate RT = Rougher tailings

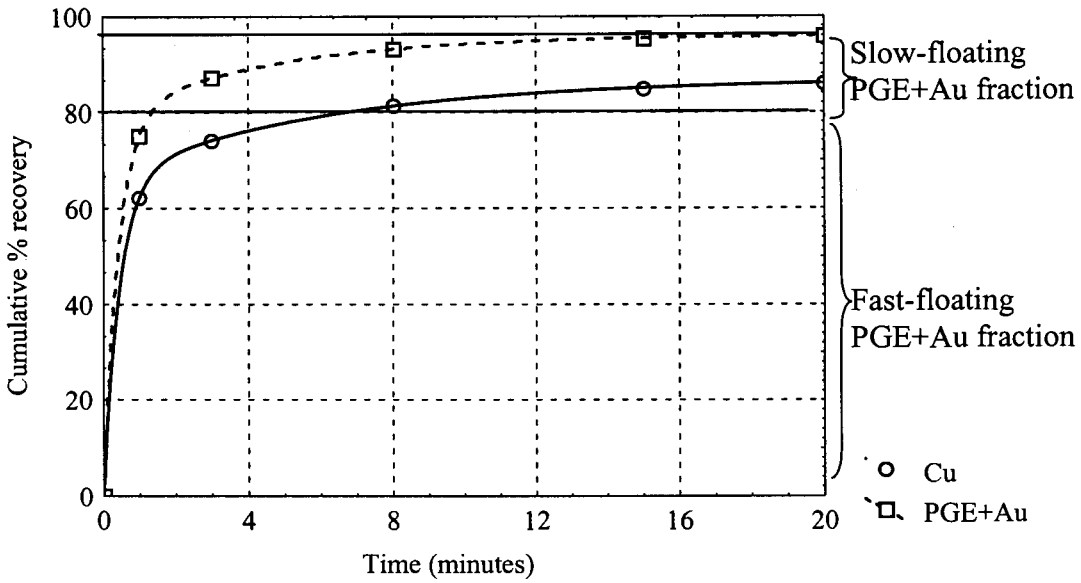

Figure 7 *Time-recovery profile for Cu and PGE+Au from sample A1. The curves were fitted to the data using the modified Kelsall model. The loss function (Loss = (Observed-Predicted)^2) of 0.018 and 0.024 for Cu and PGE+Au, respectively, indicates a good fit.*

Table 4.3 *Model parameters of three replicate tests on sample A1 for PGE+Au and 90% confidence interval using the Student t-distribution.*

PGE+Au	*U (%)*	ϕ	k_f (min^{-1})	k_s (min^{-1})
Test 1	96.1	0.17	2.39	0.22
Test 2	96.6	0.15	2.30	0.20
Test 3	95.7	0.20	2.47	0.23
Average	96.1	0.18	2.38	0.22
90% confidence interval	±0.6	±0.04	±0.12	±0.02

4.3 Chemical analysis procedures

Chemical analysis of feed material and flotation products were performed by the Analytical Services Division (ISO Guide 25 accredited) at Mintek. The techniques used are briefly outlined in Table 4.4. The precision of the analyses for the different

elements, calculated from duplicate analyses (Kaiser & Specker, 1955), is listed in Tables 4.5 and 4.6.

Table 4.4 *Chemical analysis techniques.*

Elements	**Sample preparation**	**Measurement technique**
Cr, Fe, Ca, Mg, Al, Si, Ti and Mn	Fusion with sodium peroxide followed by dissolution in HNO_3.	ICP-OES
K and Na	Dissolution in HF, HCl and $HClO_4$ followed by drying and HCl dissolution.	AA
Acid soluble Cu and Ni	Dissolution in brominated HCl and HNO_3.	ICP-OES (>500 ppm) AA (< 500 ppm)
Total Cu and Ni	Fusion with sodium peroxide followed by dissolution in brominated HCl and HNO_3.	ICP-OES (>500 ppm) AA (< 500 ppm)
Co	Fusion with sodium peroxide followed by dissolution in brominated HCl and HNO_3.	ICP-MS
Sulphur	Oxidation of sulphur to SO_2 by combustion at high temperature.	Infrared absorption
PGE+Au (Pt, Pd, Rh and Au)	Fire assay with Pb collection	ICP-MS

ICP-OES Inductively Coupled Plasma-Optical Emission Spectrometry

AA Atomic Absorption

ICP-MS Inductively Coupled Plasma-Mass Spectrometry

The lead collection technique is routinely used throughout the platinum-mining industry in South Africa to determine the platinum, palladium, rhodium and gold content (PGE+Au) of ores and plant products (Van Wyk, 1980). It is known however, that this method systematically underestimates the PGE+Au content, especially rhodium, compared with the more tedious and expensive nickel-sulphide collection

technique (Robért *et al.*, 1971; Robért *et al.*, 1997). Unfortunately, due to technical problems experienced during nickel-sulphide collection, coupled with the small amount of sample available, the analysts had to revert to the Pb collection technique for analysis of the samples produced during this study.

Table 4.5 *Analytical error calculated at the 95% confidence level for S, acid soluble Cu, total Ni , acid soluble Ni, PGE+Au (Pt+Pd+Rh+Au), Pt, Pd and Rh, over different ranges of concentration levels. N, e and E refer to the number of analyses, absolute error, and relative error respectively.*

Element	N	Range	e	E
S	38	0.01-0.10 %	± 0.01	~ 20 %
	50	0.10-1.00 %	± 0.01	~ 2 %
	6	1-10 %	± 0.11	~ 2 %
Cu a.s.	60	10-100 ppm	± 1	~ 2 %
	174	100-1000 ppm	± 13	~ 2 %
	28	0.1-1 %	± 0.02	~ 4 %
Ni t.	78	0.1-0.5 %	± 0.01	~ 4 %
Ni a.s.	156	100-1000 ppm	± 23	~ 5 %
	140	0.10-1.00 %	± 0.01	~ 2 %
PGE+Au	16	0.2-1.0 ppm	± 0.05	~ 11 %
	70	1-10 ppm	± 0.2	~ 4 %
	38	10-50 ppm	± 1	~ 5 %
Pt	34	0.1-1.0 ppm	± 0.03	~ 15 %
	76	1-10 ppm	± 0.7	~ 14 %
	78	10-100 ppm	± 3	~ 6 %
Pd	50	0.1-10 ppm	± 0.02	~ 9 %
	88	1-10 ppm	± 0.3	~ 8 %
	52	10-50 ppm	± 1.3	~ 5 %
Rh	62	0.1-1.0 ppm	± 0.06	~ 15 %
	106	1-15 ppm	± 0.59	~ 9 %

a.s.= acid soluble *t.=total*

Table 4.6 *Analytical error calculated at the 95% confidence level for Cr, Fe, Mg, Al, Si, Ca and Ti (expressed as oxides) over different ranges of concentration levels. N, e and E refer to the number of analyses, absolute error, and relative error respectively.*

Oxide	N	Range	e	E
Cr_2O_3	82	10-35 %	0.26 %	~ 1 %
Fe_2O_3	70	10-30 %	0.27 %	~ 1 %
MgO	68	10-20 %	0.10 %	~ 1 %
Al_2O_3	68	10-20 %	0.15 %	~ 1%
SiO_2	80	10-35 %	0.16 %	~ 1 %
CaO	64	2-6 %	0.1 %	~ 3 %
TiO_2	58	0.2-1.0 %	0.0 %	< 1 %

4.4 Comparison of calculated and analysed feed grades

A further indication of the quality of the flotation results (mass recoveries and chemical analyses combined) is given by the comparison of analysed and calculated feed grades. The latter value is back-calculated from the mass distributions and chemical analyses of flotation products. In Table 4.7 the analysed and calculated PGE+Au, platinum, palladium and rhodium feed grades of three sub-samples of sample A1 are compared. In the case of PGE+Au, platinum and palladium, the analysed and calculated feed values tally well, with the percentage difference between the two values consistently below 5 per cent. In the case of rhodium the differences are larger (31, 22 and 24 per cent for the three sub-samples), due to the increased error associated with the lower concentration levels of this element.

Table 4.7 *A comparison of calculated and analysed PGE+Au, Pt, Pd and Rh feed grades for three sub-samples of sample A1.* [1] *= feed grades calculated from mass distributions and analysed grades of flotation product samples* [2] *= analysed feed grade* [3] *= % difference*

A1 Test A	*Dry mass (g)*	*Dry mass (g) cum.*	*Mass Distr. %*	*Mass Distr. % cum.*	*PGE+Au g/t*	*PGE+Au g/t cum.*	*Pt cont. g/t*	*Pt cont. g/t cum.*	*Pd cont. g/t*	*Pd cont. g/t cum.*	*Rh cont. g/t*	*Rh cont. g/t cum.*
RC1	218.00	218.00	3.64	3.64	108.84	108.84	66.25	66.25	29.03	29.03	11.63	11.63
RC2	141.20	359.20	2.36	5.99	26.45	76.45	16.00	46.50	7.44	20.54	2.91	8.20
RC3-5	292.90	652.10	4.89	10.88	9.45	46.36	5.66	28.15	2.77	12.56	1.02	4.97
RT	5339.60	5991.70	89.12	100.00	0.24	**5.26**[1]	0.13	**3.18**[1]	0.09	**1.44**[1]	0.02	**0.56**[1]
						5.06[2]		**3.08**[2]		**1.42**[2]		**0.43**[2]
						4[3]		**3**[3]		**1**[3]		**31**[3]
A1 Test B	*Dry mass (g)*	*Dry mass (g) cum.*	*Mass Distr. %*	*Mass Distr. % cum.*	*PGE+Au g/t*	*PGE+Au g/t cum.*	*Pt cont. g/t*	*Pt cont. g/t cum.*	*Pd cont. g/t*	*Pd cont. g/t cum.*	*Rh cont. g/t*	*Rh cont. g/t cum.*
RC1	231.30	231.30	3.86	3.86	101.33	101.33	58.70	58.70	29.40	29.40	10.38	10.38
RC2	154.50	385.80	2.58	6.44	24.03	70.37	14.15	40.86	7.00	20.43	2.55	7.24
RC3-5	298.50	684.30	4.98	11.41	9.00	43.60	5.28	25.34	2.80	12.74	0.85	4.46
RT	5310.70	5995.00	88.59	100.00	0.21	**5.16**[1]	0.13	**3.01**[1]	0.08	**1.53**[1]	0.02	**0.53**[1]
						5.06[2]		**3.08**[2]		**1.42**[2]		**0.43**[2]
						2[3]		**2**[3]		**7**[3]		**22**[3]
A1 Test C	*Dry mass (g)*	*Dry mass (g) cum.*	*Mass Distr. %*	*Mass Distr. % cum.*	*PGE+Au g/t*	*PGE+Au g/t cum.*	*Pt cont. g/t*	*Pt cont. g/t cum.*	*Pd cont. g/t*	*Pd cont. g/t cum.*	*Rh cont. g/t*	*Rh cont. g/t cum.*
RC1	224.40	224.40	3.74	3.74	99.37	99.37	60.53	60.53	29.38	29.38	10.20	10.20
RC2	136.10	360.50	2.27	6.01	26.50	71.86	16.30	43.83	7.20	21.01	2.80	7.41
RC3-5	280.40	640.90	4.68	10.69	10.80	45.15	6.30	27.41	3.10	13.17	1.27	4.72
RT	5354.60	5995.50	89.31	100.00	0.25	**5.04**[1]	0.16	**3.07**[1]	0.09	**1.49**[1]	0.03	**0.53**[1]
						5.06[2]		**3.08**[2]		**1.42**[2]		**0.43**[2]
						0[3]		**0**[3]		**5**[3]		**24**[3]

4.5 Mineralogical techniques

4.5.1 X-ray diffraction (XRD)

Prior to analysis, samples were pulverised in a Siebtechnik vibratory ring mill for 2 minutes. This was followed by a 10 minute grinding session in the McCrone Micronising Mill to minimise particle-size effects during analysis. A Siemens D-500 diffractometer using CuKα radiation was employed. The sample was scanned over the range of 4 to 76° 2θ at a step size of 0.02° 2θ and a counting time of 1 second per step. This configuration gives a lower detection limit of approximately 3 to 4 volume per cent of the crystalline phases present in the sample. In the case of layer silicates such as talc and chlorite, the detection limit can be expected to be lower due to preferred orientation of these phases.

X-ray diffraction was used to investigate major variations in the mineralogy of the ore and product samples, particularly with regard to the layer silicates such as talc, chlorite and amphibole. The low concentrations of these minerals, combined with their tendency for preferred orientation, make quantification of these phases almost impossible task. Consequently, X-ray diffractograms were evaluated in a purely qualitative manner.

4.5.2 Preparation of polished sections

The stereological principles on which the analysis of polished sections are based are valid only if the features to be measured are in random plane sections, and are sampled representatively. Sample preparation frequently represents the main source of error in measurements on polished sections (Petruk, 1976; Rowlands *et al.*,1991). To minimise the error introduced during sampling, a rotary sample splitter was used to ensure that sub-samples were obtained in a representative manner.

One of the problems during preparation of polished sections of powdered samples is the segregation of particles of different shape, size and density. To counteract the effect of segregation, the following procedures were followed: The sample is mixed with Araldite resin in a small pill-vial and then left to cure at 60°C. The result is a small cylindrical piece of araldite (~1cm diameter by 0.5 cm length) containing the

sample particles. This cylinder is then cut parallel to the direction of settling with a diamond saw. The resulting sliver is remounted in Perspex rings and polished according to standard procedures. To obtain data on a representative sample, measurements have to be made on continuous traverses, parallel to the direction of settling (Bushell, 1987; Oosthuyzen, 1987).

It is essential that sample contamination, such as that due to the introduction of brass and lead from sawing and polishing equipment for instance, or cross-contamination between samples during sample handling, is avoided. In addition, artefacts, such as air bubbles, can cause electrostatic charging of the surface, leading to errors during image-analysis measurements.

The conventional approach is to screen each sample into several size fractions, followed by weighing, chemical analysis, and image-analysis measurements on polished sections of each size fraction (Petruk *et al.*, 1986; Van den Heever, 1995). However, in the case of the samples under investigation, it was decided to perform the measurements on unscreened samples. Furthermore, no attempt was made to avoid touching grains by the addition of a filler material, such as graphite (Miller *et al.*, 1982; Jackson *et al.*, 1984). The reasons for this approach are as follows: As a result of the low concentration levels at which the base-metal sulphides and PGE minerals are present in these samples, very little concentrate is generated during flotation. To generate enough flotation concentrate to allow chemical and mineralogical analysis of several size fractions, would necessitate the flotation of several more kilograms of sample. Dilution of samples by addition of a filler material, would mean that a larger number of polished sections have to be scanned. If enough filler is added for effective separation of touching grains in a fine-grained fraction fraction, several times the area has to be scanned to find the same number of PGE mineral grains, increasing analysis time per sample from days to weeks.

4.5.3 Optical microscopy

Polished sections of crushed feed, milled feed, and flotation products were examined under the ore microscope (Zeiss Axioplan) to identify the major ore minerals and their

relationships. A number of thin sections were examined to determine the identity and mode of occurrence of the silicate minerals.

4.5.4 Scanning-electron microscopy (SEM)- Energy-dispersive X-ray spectrometry (EDS)

Scanning electron microscopy (Cambridge S360 and LEO S440) coupled with energy-dispersive X-ray analysis (Link AN 10000 and Oxford Isis) was used as an aid to mineral identification. Full quantitative to semi-quantitative EDS analysis was carried out on a number of silicate minerals. The elements analysed for, and the standards used, are listed in Table 4.8.

Analytical conditions were 20 kV accelerating voltage, a beam current of 3 nA, and a counting time of 50 seconds. A $\phi(\rho Z)$ matrix correction procedure was applied to the raw data. Under these conditions the level of precision for all elements, at concentration levels down to 0.5 mass per cent, was less than ±0.1 mass per cent (99% confidence level). Secondary standards of enstatite, diopside, hypersthene, hornblende and anorthite were analysed to ensure the level of accuracy. Beam stability was monitored by measuring the sample current every 15 minutes.

Table 4.8 *Elements (expressed as oxides) analysed for and standards used during quantitative EDS analysis of silicate minerals.*

Element	**Standard**
Na_2O	Albite
MgO	MgO Periclase
Al_2O_3	Al_2O_3 Corundum
SiO_2	SiO_2 Quartz
K_2O	Microcline
CaO	$CaSiO_3$ Wollastonite
TiO_2	TiO_2 Rutile
Cr_2O_3	Cr_2O_3
MnO	Mn_3O_4 Hausmanite
Fe_2O_3	Fe_2O_3 Hematite
NiO	NiO

4.5.5 Electron-microprobe analysis

Chromite

Quantitative electron-microprobe analysis using WDS (wavelength dispersive X-ray spectrometry) on chromite was carried out on an ARL-SEMQ instrument. The following oxides were analysed for: SiO_2, TiO_2, V_2O_3, Al_2O_3, Cr_2O_3, FeO, MnO, NiO, CoO, Cu_2O, ZnO, MgO and CaO. Standards used were pure oxides except in the case of Ca for which diopside ($CaMgSi_2O_6$) was used.

Duplicate analyses were obtained for each grain. The operating conditions were 15 kV accelerating voltage and 35 nA beam current. Counting times were 50 seconds on background and 100 seconds on the peak. A $\phi(\rho Z)$ matrix correction procedure was applied to the raw counting data. The detection limits under these conditions are listed in Table 4.9.

Table 4.9 *Detection limits (D.L.) (99% confidence level) and precision (95% confidence level) for oxides analysed. Analytical precision was calculated at the 95% confidence level from duplicate analyses of 155 grains (Kaiser & Specker, 1955).*

Oxide	D.L. (ppm)	Range (wt%)	Precision (wt%)	X-ray line
MnO	230	0.23 to 0.32	±0.03	K_α
NiO	300	0.06 to 0.20	±0.03	K_α
ZnO	500	0.00 to 0.19	±0.05	K_α
V_2O_3	1040	0.17 to 0.64	±0.10	K_α
CoO	740	0.00 to 0.12	±0.05	K_α
Cu_2O	1170	0.00 to 0.17	±0.06	K_α
MgO	360	7.67 to 11.03	±0.39	K_α
Al_2O_3	370	13.50 to 18.70	±0.23	K_α
FeO	100	26.41 to 32.06	±0.34	K_α
SiO_2	90	0.00 to 3.89	±0.62	K_α
TiO_2	80	0.49 to 5.75	±0.51	K_α
Cr_2O_3	70	39.86 to 46.26	±0.54	K_α
CaO	70	0.00 to 0.13	±0.00	K_α

Base-metal sulphides and PGE minerals

Quantitative electron-microprobe analyses of PGE minerals and base-metal sulphides were carried out on a JEOL-Superprobe 733 with a Voyager 3 upgrade WDS/EDS.

Base-metal sulphides

Wavelength dispersive X-ray analysis was used for the determination of Pt, Pd, Rh, Cu, Fe, Ni, Cu, Co and S in pentlandite, chalcopyrite, pyrite, pyrrhotite, millerite and siegenite.

The following standards were used:

Pure metal for Rh.
$Pt_{0.7}Pd_{0.3}S_{1.0}$ for Pt.
PdS for Pd.
Co_9S_8 for Co.
NiS for Ni.
FeS for Fe and S in all phases except chalcopyrite.
$CuFeS_2$ for Cu and Fe in chalcopyrite.

The operating conditions were an accelerating voltage of 15 kV and a beam current of 30 nA. Counting times were 200 seconds on the peak and 200 seconds on background for the platinum-group elements and 30 seconds for the major elements. A PROZA matrix correction procedure was applied to the raw counting data. The detection limits and reproducibility under these conditions are reported in Tables 4.10 and 4.11.

The purpose of these analyses was twofold - firstly to chemically characterise the base-metal sulphides in terms of their major components, and secondly to investigate the presence of trace amounts of platinum, palladium, and rhodium in solid solution form in these phases. At least two analyses were performed on each grain - the reported values are the mean values of these two analyses. If only one of the analyses indicated the presence of significant platinum, palladium or rhodium, additional points were analysed. Isolated high values were assumed to be due to the presence of discrete PGE minerals either too small to be recognised on the backscattered-electron image, or below the surface of the polished section.

Table 4.10 *Analytical reproducibility of S, Fe, Cu, Co and Ni in pyrrhotite, pentlandite, chalcopyrite, pyrite, millerite and siegenite calculated at the 95% confidence level from duplicate analyses (Kaiser & Specker, 1955). n = the number of grains on which the calculations were based.*

	Pyrrhotite	**Pentlandite**	**Chalcopyrite**	**Pyrite**	**Millerite**	**Siegenite**
n	42	55	53	52	29	7
S	38.10 ±0.58	33.26 ±0.49	34.91 ±0.67	52.45 ±0.83	35.27 ±0.58	41.70 ±0.84
Fe	61.41 ±0.96	33.81 ±0.53	30.44 ±0.59	44.69 ±0.95	1.27 ±0.16	1.64 ±0.97
Ni	0.10 ±0.39	31.75 ±0.62	0.04 ±0.11	2.57 ±0.41	62.24 ±0.84	32.78 ±1.19
Co	0.07 ±0.05	0.58 ±0.07	0.04 ±0.05	0.68 ±0.62	0.82 ±0.08	21.74 ±0.64
Cu	0.02 ±0.04	0.05 ±0.07	34.04 ±0.79	0.33 ±0.05	0.05 ±0.09	0.03 ±0.04

Table 4.11 *Detection limits of Pt, Rh, Pd and Ru in ppm in pyrrhotite, pyrite, chalcopyrite, pentlandite and millerite calculated at the 99% confidence level.*

	Pyrrhotite	**Pyrite**	**Chalcopyrite**	**Pentlandite**	**Millerite**	**X-ray line**
Pt	295	320	315	300	300	M_α
Rh	225	200	210	225	215	L_α
Pd	285	265	290	295	285	L_β
Ru	210	205	210	205	215	L_α

It should be noted that, in the case of trace element analysis, inaccuracies are introduced when standard correction procedures are applied due to differences in the concentration levels of the relevant elements between calibration standards and the sample being analysed. As no suitable calibration standards of sulphide with trace amounts of PGEs were available, the determination of trace amounts of PGEs in base-metal sulphides should be considered semi-quantitative.

PGE minerals

The major objective of the analysis of the PGE minerals was mineral identification. No attempt was made to investigate differences in PGE mineral composition between samples. Due to the small grain sizes of the PGE minerals, duplicate analyses could not be obtained on all grains.

The following elements were analysed for by wavelength dispersive X-ray analysis: As, S, Ru, Rh, Pd, Te, Pt, Hg, Pb, Bi, Fe, Co, Ni and Cu. The operating conditions were accelerating voltage 20kV, beam current 20 nA, and counting time 20 seconds peak count. A Duncumb-Reed correction procedure was applied to the raw counting data.

4.6 Image-analysis techniques

4.6.1 Introduction

Microscopic investigations play a crucial role in the development and monitoring of metallurgical processes. Traditionally, such investigations were carried out by mineralogists who used their training and experience to make observations regarding aspects such as mineral identification, the modal proportions of minerals, their grain sizes, shapes, associations and degree of liberation of valuable constituents. These observations are generally made on polished sections of ores and mineral processing products. Over the years, researchers (amongst others Chayes, 1956; 1963; Jones & Shaw, 1973; Petruk, 1976; 1986; 1988a; 1993; 1994; Gateau, 1978; Gateau & Prevosteau, 1978; Oosthuyzen, 1983; 1987) have proposed and used various methods and techniques to quantify microscopic observations, eventually leading to the development of automated image-analysis techniques.

4.6.2 Application to UG2 feed and product samples – general principles

The Leica Cambridge morphochemical-analysis system at Mintek consists of a Quantimet 570 image analyser fully integrated with a Stereoscan 360 SEM and a Link AN 10000 EDS system (Figure 8). Using the programming language, QBASIC, this system can be programmed to automatically scan across polished sections, and to perform image-analysis routines tailor-made for different applications. These include quantitative information on the modal composition of the samples, as well as grain-size distributions and mode of occurrence of specific minerals. All the image analysis routines used during this investigation consist of various combinations of a number of basic steps:

Image generation and transfer

Backscattered-electron images generated by the SEM are used as input to the image analyser. Conversion of the analogue image into a digital image results in a grid of 512 x 512 pixels (or picture elements), each with a specific grey level value between 0 (black) and 255 (white). ‡

Figure 9 represents a typical backscattered-electron image of crushed UG2 ore. In this image different mineral phases show up with different shades of grey (or grey levels), such that phases with a high weighted mean atomic number (and consequently high backscattered-electron coefficient, $\bar{\eta}$ (Reed, 1975; Heinrich, 1981)) like the PGE minerals, appear very bright, while phases with a low weighted mean atomic number, such as silicates, are dark.

Figure 8 *The Leica Cambridge morphochemical-analysis system.*

‡ Note that this information is specific to the instrumentation used.

Image segmentation

Before image-analysis measurements can be performed on such a backscattered-electron image, it needs to be converted into a series of binary images in which each pixel can have only one of two states - on or off (background or interest). Such a binary image is produced by segmentation of the grey image into regions that are characterised by a specific property, in this case, grey level (Figure 10) (*Anon*, 1985).

An objective method of grey-level segmentation is provided by the grey-level histogram, produced by plotting the number of pixels with each specific grey level in an image (or series of images) against grey level. Figure 11 represents the grey-level histogram of the image in Figure 9. Apart from a peak representing the mounting resin, two major peaks can be seen, a silicate peak between grey level 28 and 52, and a chromite peak stretching from grey level 88 to 120. The area between grey level 118 and 198 (enlarged in Figure 12) comprises a number of overlapping peaks representing different sulphide minerals. The small peak visible at the far right-hand side of the histogram in Figure 12 (grey level 240 to 255) represents braggite.

Overlapping grey levels is one of the biggest problems faced during segmentation of such images. The calculated weighted mean atomic numbers and backscattered-electron coefficients for most of the phases found in the samples investigated, are listed in Table 4.12. Measured mean grey-level values for some of these phases are also listed. It is clear that many of the phases present in samples derived from UG2 ore have similar backscattered-electron coefficients and grey-level values (pyrite & magnetite and pentlandite & chalcopyrite for instance).

Note that the relationship between mean atomic number and backscattered-electron coefficient (and consequently grey level) is not linear (Figure 13). Consequently, for the heavier phases, a difference in mean atomic number between two phases does not necessarily signify a measurable difference in backscattered-electron intensity (or grey level). Compare for instance the mean atomic numbers and backscattered-electron intensities of brass and laurite.

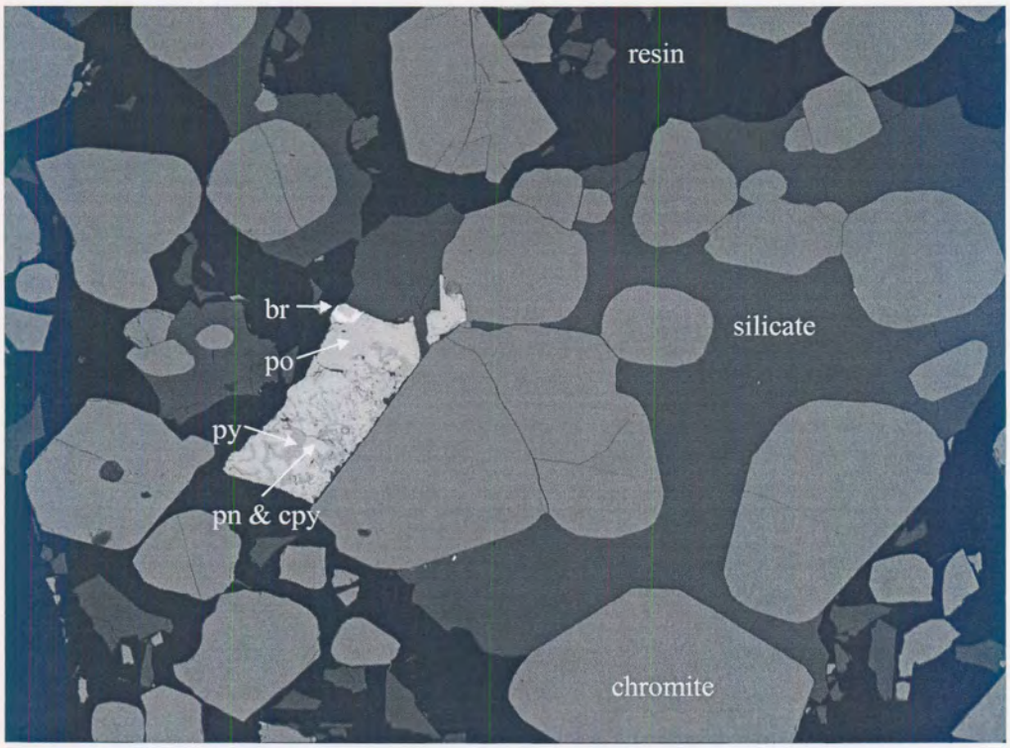

Figure 9 *Backscattered-electron image of UG2 ore containing, in order of increasing grey level: mounting resin → silicates → chromite → pyrite (py) → pyrrhotite (po) → chalcopyrite (cpy) = pentlandite (pn) → braggite (br).*

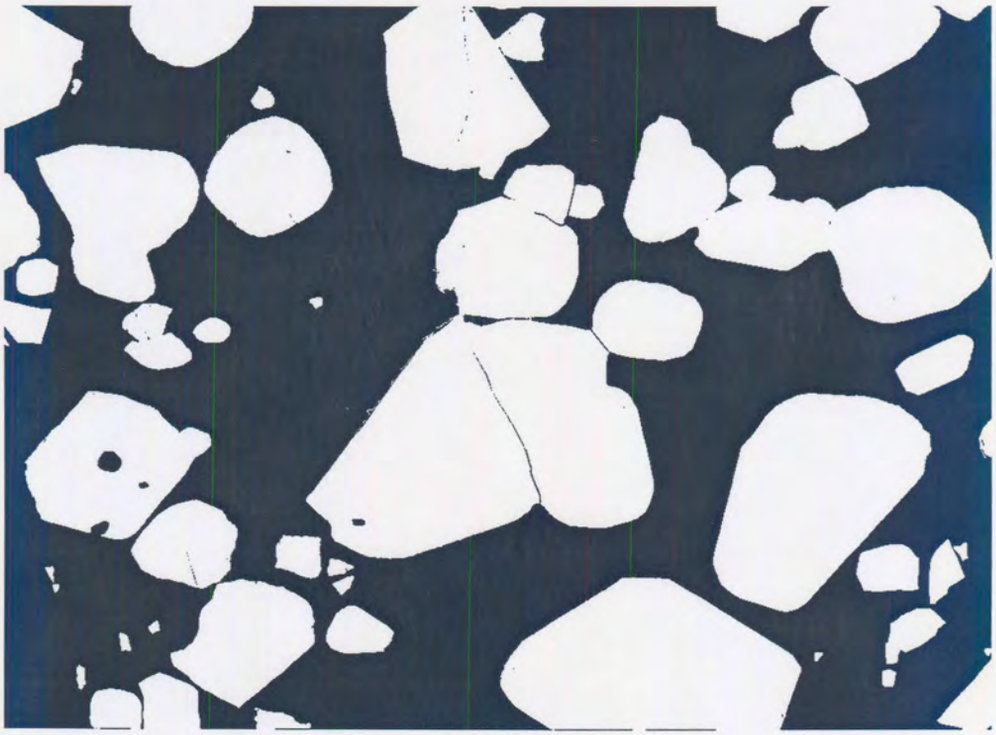

Figure 10 *Binary image of chromite in Figure 9.*

In addition, as can be seen from Figures 11 and 12, the histogram peak for any specific phase is often quite broad, comprising a range of grey-level values. This can be attributed to variations in chemical composition, both between and within grains, as well as artefacts introduced during sample preparation, grain-edge effects (especially in the case of small grains), and the quality and stability of the backscattered-electron signal.

Image processing techniques and the integration of image analysis with EDS analysis make it possible to resolve the problem of overlapping grey levels to a certain extent.

Table 4.12 *Weighted mean atomic number ($\bar{Z}$), backscattered-electron coefficient ($\bar{\eta}$) and measured mean grey level (m.g.l.) of commonly found phases present in UG2 ore and product samples arranged in order of ascending $\bar{Z}$. Where possible, calculations of weighted mean atomic numbers and backscattered-electron coefficients were based on electron-microprobe analyses of the phases.*

Phase	$\bar{Z}$	$\bar{\eta}$	***m.g.l.***
Talc	11.0	0.14	30
Anorthite	11.6	0.12	38
Bronzite	12.5	0.18	52
"Normal" chromite	17.4	0.20	93
"Sintered" chromite	18.4	0.21	106
Pyrite	20.7	0.23	154
Magnetite	21.0	0.23	
Pyrrhotite	22.1	0.24	174
Millerite	22.4	0.25	
Pentlandite	23.3	0.25	186
Chalcopyrite	23.5	0.25	188
Stainless steel	25.7	0.28	
Brass	29.4	0.31	
Laurite	33.1	0.31	
Vysotskite	39.1	0.35	
Malanite	48.3	0.36	
Braggite	54.5	0.39	248
Cooperite	68.0	0.44	
Pt-Fe alloy	72.2	0.46	
Galena	73.2	0.45	

See Appendix A for the method of calculation of mean atomic numbers and backscattered-electron coefficients.

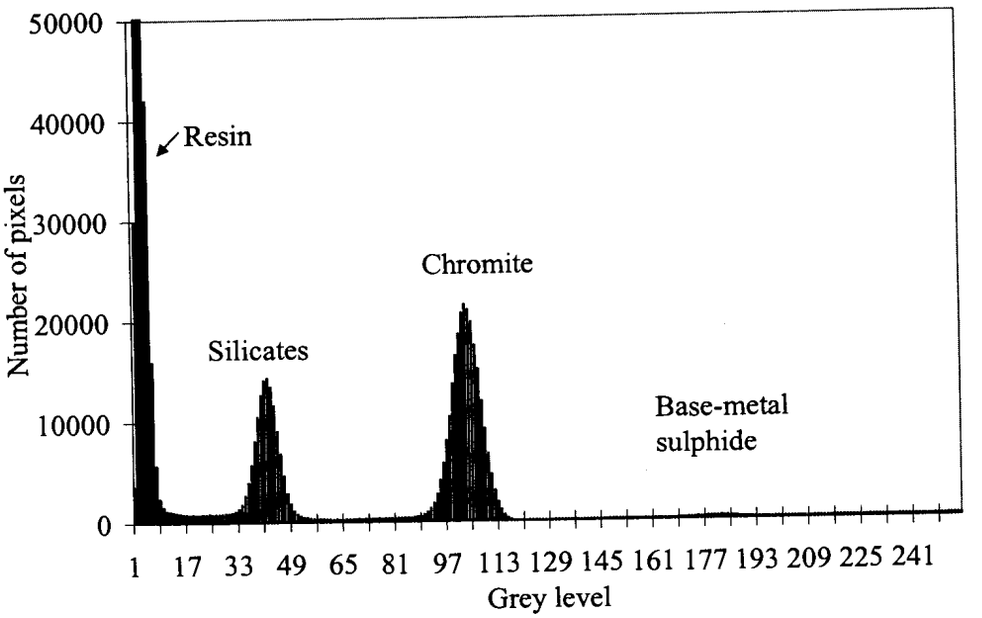

Figure 11 *Grey-level histogram of a backscattered-electron image of UG2 ore.*

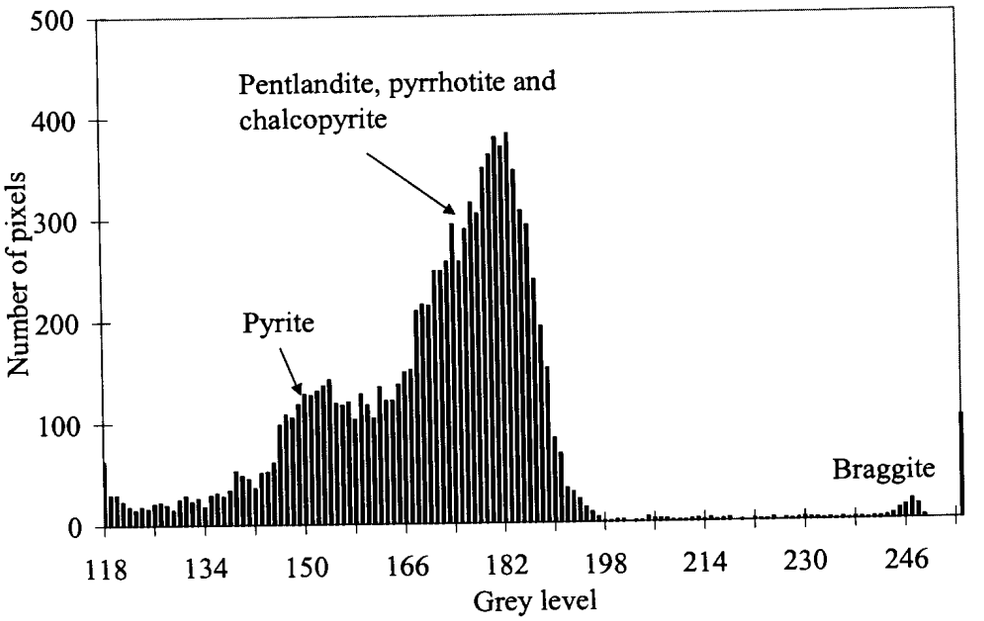

Figure 12 *Grey-level histogram from grey level 116 to 255.*

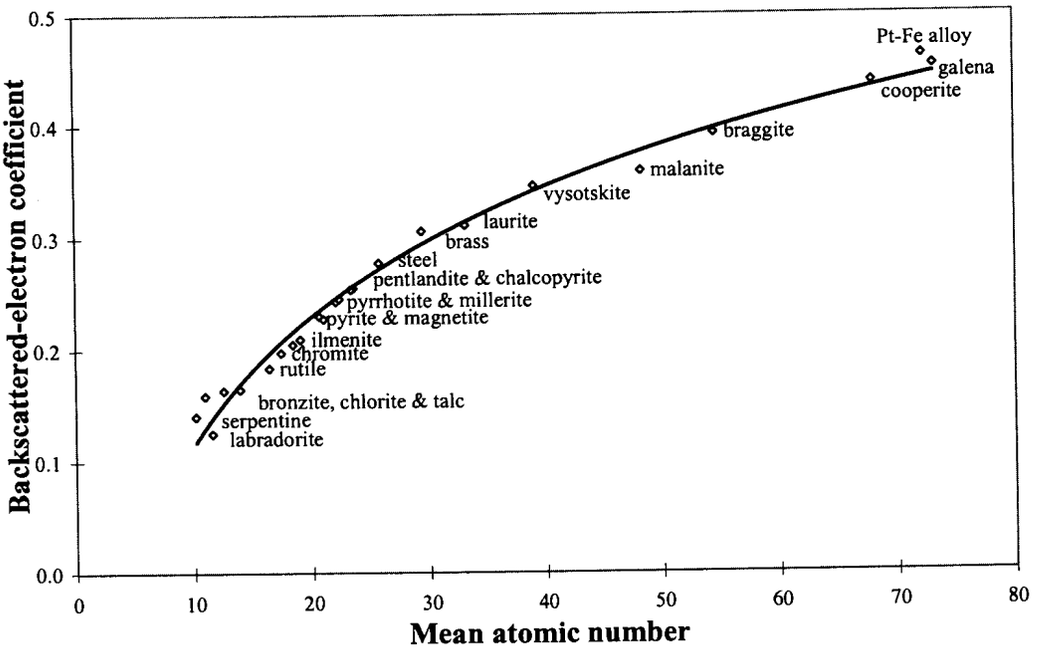

Figure 13 *Graph of weighted mean atomic number ($\bar{z}$) against backscattered-electron coefficient ($\bar{\eta}$) for phases in UG2 flotation feed and products.*

Image processing

Image processing operations can be carried out both on grey and binary images. Grey-level image processing can be used to simplify or improve an image prior to analysis, by eliminating irrelevant data such as that produced by electronic noise, or artefacts introduced during preparation of polished sections.

The effect of grey-level processing on the image in Figure 9 is illustrated in Figure 14. The image was subjected to a series of grey-level processing operations to first produce a less noisy image, followed by a sharpening of the grain-edges. After grey-level processing, the peaks on the histogram are clearly better defined than before processing.

Binary image processing is significantly faster than grey-level processing. However, since a binary image contains less information than a grey image, errors introduced during image segmentation can be compounded during binary image processing. A

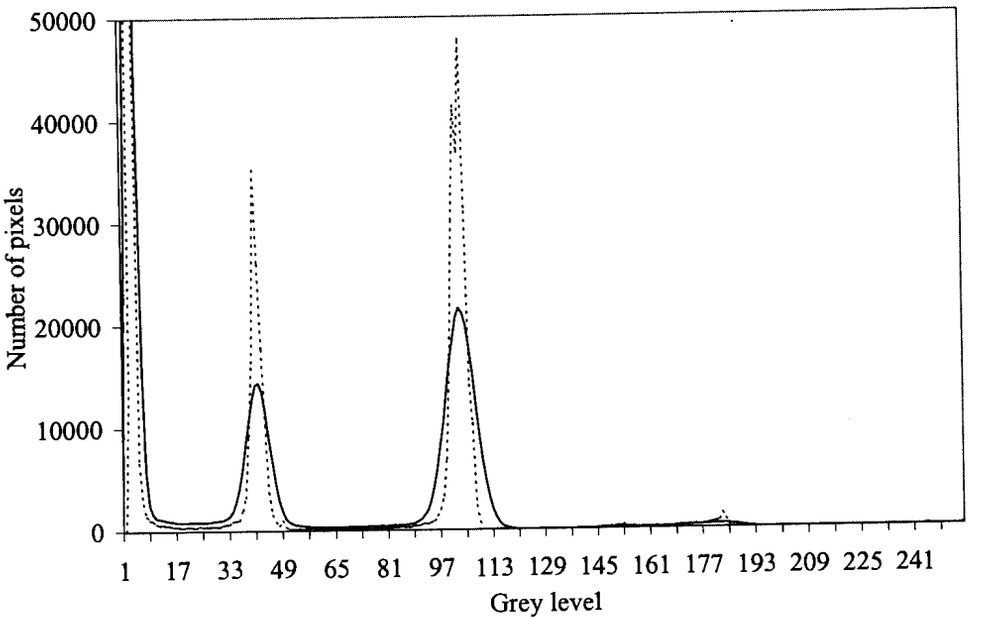

Figure 14 *Grey-level histogram of the image in Figure 9 before (solid line), and after (broken line) grey image processing.*

variety of binary image processing tools are available to perform functions such as separating of touching particles and elimination of polishing imperfections. The use of some binary image processing functions during analysis of UG2 samples is illustrated in Figure 15.

Image analysis combined with EDS analysis

In some cases, no amount of image processing will make it possible to discriminate between two phases based on grey level alone. In such cases the grey-level data can be combined with chemical data obtained by EDS analysis. This does, however, increase the analysis time substantially. The relatively poor spatial resolution of the EDS analysis compared to that of the backscattered-electron signal is a further disadvantage (Jones & Shaw, 1973; Rowlands *et al.*, 1991; Gu, 1998).

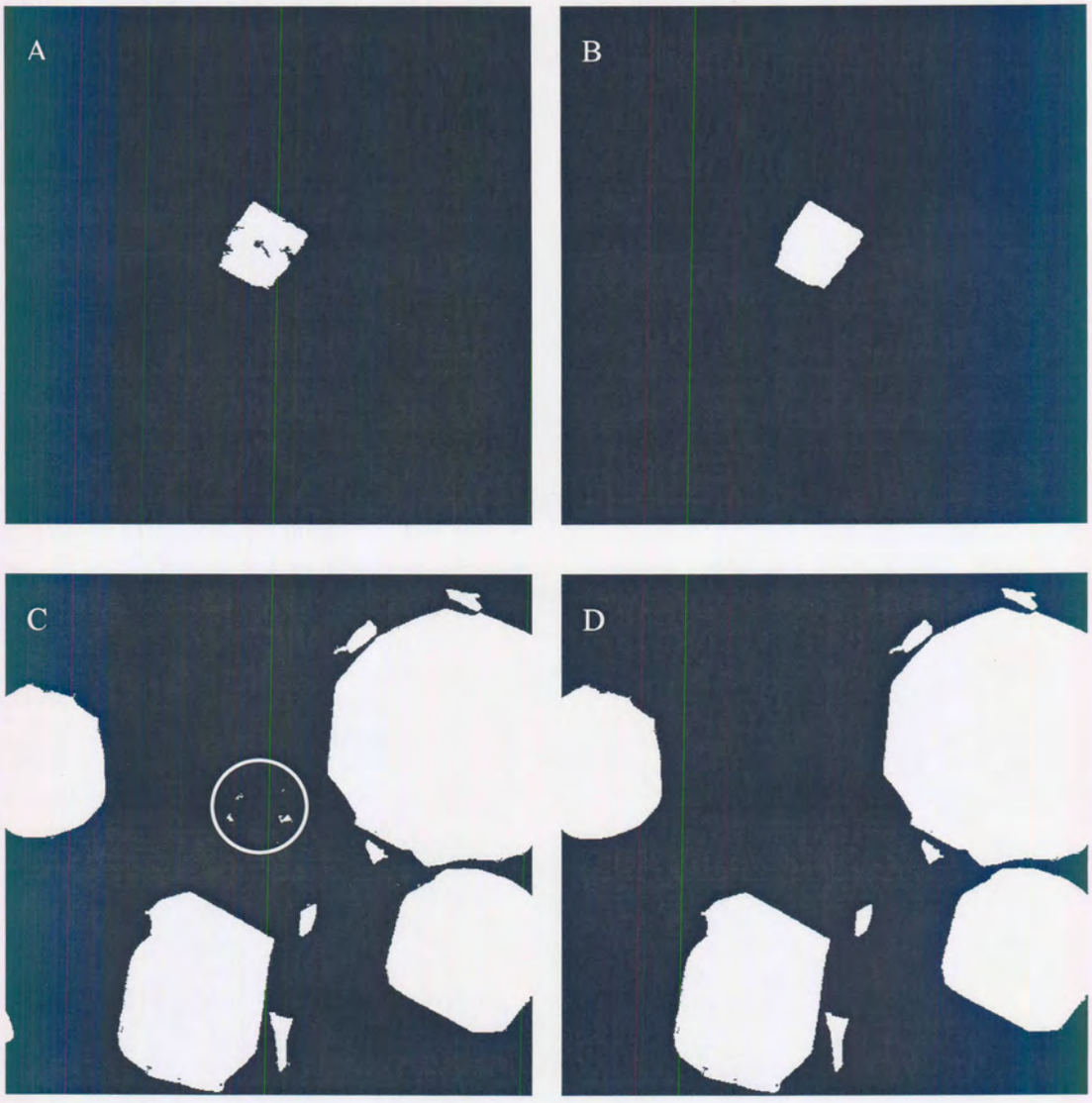

Figure 15 *Examples of binary image processing used on UG2 samples.*

A. Binary image of a sulphide grain. Note the presence of "holes" in the grain caused by polishing imperfections.

B. Binary image of the same sulphide grain after binary image processing to fill the holes.

C. Binary image of chromite - note the presence of artefacts in the circled area.

D. Binary image of chromite after binary image processing to remove artefacts.

Measurement

Once a binary image of each phase of interest in a field has been successfully created, the image is ready for quantification. Provided a statistically valid number of measurements are made, the relative amounts (modal composition), size distribution and mode of occurrence (mineral association and degree of liberation) of specific phases in a sample can be estimated.

Modal analysis

The modal composition of a sample can be estimated from point, line or area measurements on randomly sectioned polished surfaces (Chayes, 1956; DeHoff & Rhines, 1968; Weibel, 1980; Jones, 1987). For example, the number of pixels in the binary image of chromite (see Figure 10), calculated as a percentage of the total number of pixels for all minerals, gives the area proportion (which is equivalent to volume proportion) of chromite in the sample. The volumetric proportion of a phase can be readily converted to mass proportion if the relative densities of the phases are known.

Grain-size distribution

Provided all touching grains have been separated (either physically during sample preparation or by image-processing techniques), grain-size distributions can be derived from line or area measurements on polished sections. Since grains may be cut across their extremities and appear smaller than their true size, these measured size distributions produce biased estimates of the true, three-dimensional sizes of the grains. Obtaining a true grain-size distribution from measurements made on polished sections is one of the most difficult problems of stereology. No attempt was made to apply stereological corrections to the grain-size data collected during the course of this study.

In this report grain size will be expressed as equivalent circle diameter ($ECD = 2 * \sqrt{Area / \pi}$, *i.e.* the diameter of a circle with the same area as that of the measured grain).

For more in-depth information on grain-size measurements and three-dimensional reconstruction the reader is referred to DeHoff (1965), Saltikov (1967), DeHoff & Rhines (1968), Underwood (1970), Petruk (1976), King (1978), Weibel (1980), and Vander Voort (1984).

Degree of liberation

Degree of liberation can be defined as the extent to which valuable phases have been separated from gangue during comminution, and can be measured either by linear intercepts (e.g. King, 1993; 1994b) or area measurements (Petruk, 1993; Petruk & Lastra, 1995). Estimations of degree of liberation based on measurements on polished sections yield apparent values, because only two dimensions of three-dimensional particles are exposed. Consequently, the number of liberated grains will always be overestimated because a number of composite particles will have been sectioned in such a way that they appear free.

Various mathematical models have been proposed for converting apparent liberation to absolute liberation (King, 1979; Lin *et al.*, 1984; Barbery, 1992a; 1992b; King, 1993; Leigh, 1993; King, 1994a; 1994b; King & Stirling, 1994; Woollacott & Valenta, 1996; Gay, 1999). However, the mechanics of ore breakage during milling is still poorly understood. Most models for predicting liberation are based on an assumption of non-preferential or random breakage, i.e. breakage is independent of texture, occurring across grain boundaries and by chipping edges off particles (King, 1979; Leigh, 1993; King, 1994; Gay, 1999, Wei & Gay, 1999). This approach has been questioned by authors such as Petruk (1988b), Ferrara *et al.* (1989), Laslett *et al.* (1990), Woollacott & Valenta (1996) and Thomas & Filipov (1999), as many ores, including the UG2 chromitite, are characterised by preferential breakage along grain boundaries, fractures, or layers and veinlets of softer minerals.

For the purpose of this project, the apparent degree of liberation of PGE minerals and base-metal sulphides from UG2 ore was calculated by measuring the area per cent of

4.6.3 Modal analysis

Major phases (base-metal sulphide, oxide and silicate)

The relative proportions of sulphide, oxide (almost exclusively chromite) and silicate in the samples were estimated by areal analysis with phase discrimination based on backscattered-electron intensity.

Individual base-metal sulphides

Measurement of the relative amounts of individual sulphides was hampered by overlapping grey levels (see Table 4.12 and Figures 12 & 13). Consequently, the modal amounts of the base-metal sulphide minerals were determined by automated EDS point analysis along a grid pattern, superimposed on the binary image of all minerals with grey levels corresponding to that of the base-metal sulphides. The grid pattern was determined by the estimated grain size of the sulphides, ensuring that only one point was measured on each grain, thus improving the statistical reliability of the results. The EDS residence time per point was 1s. EDS analysis was only performed where the grid intersected sulphide. The relative intensities of raw X-ray counting data were used to classify points.

Statistical considerations – modal analysis of major phases based on grey level

Crushed feed samples

Test measurements were done on 25 polished sections of crushed sample A1. Based on the results of these measurements, the percentage relative error in the modal amounts of base-metal sulphide, oxide and silicate at the 95% confidence level was estimated (Simon & Bruce, 1991) for 1 to a 1000 polished sections (Figure 16). The results indicate that measurements on five polished sections are sufficient to ensure a relative error of less than 5 per cent for both chromite (at 55.4 area per cent) and silicate (at 44.5 area per cent). It is estimated that at the low concentration levels at which the sulphide minerals are present (~0.10 area per cent), ~100 polished sections would have to be measured to ensure a relative error of less than 10 per cent. For practical reasons it was decided to carry out these measurements on ~5 polished

sections of each crushed sample, giving a relative error of ~40 per cent for the total base-metal sulphide.

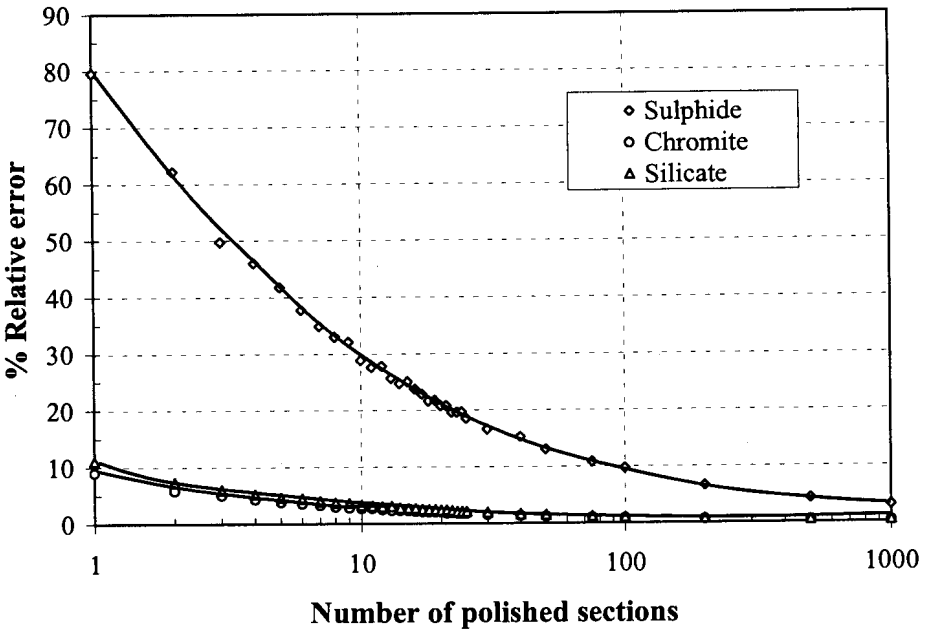

Figure 16 *% Relative error of the modal estimates of base-metal sulphide, chromite and silicate in crushed UG2.*

Milled feed

Figure 17 shows the results of similar tests on UG2 ore milled to 80% <75µm. Comparison of figures 16 and 17 illustrates the homogenising effect of milling, with a higher degree of precision obtained during measurements on the milled samples.

The measured value of base-metal sulphide is 0.16 area per cent in the milled sample compared to 0.10 area per cent in the crushed sample. Careful monitoring of the measurements indicated that the amount of base-metal sulphide in the milled feed is consistently estimated at a higher value, indicating that the difference is not merely a statistical artefact. The discrepancy is mostly caused by the introduction of stainless steel particles during milling. Even though the average backscattered-electron intensity of stainless steel is slightly higher than that of the base-metal sulphides, the small particle sizes of both stainless steel and base-metal sulphide makes it difficult to discriminate between the two types of particle based on backscattered-electron

intensity alone. Image analysis combined with EDS analysis indicate a corrected base-metal sulphide value of 0.08 area per cent.

Statistical considerations – base-metal sulphide modal analysis using EDS analysis

From test measurements on 30 polished sections of crushed sample A1, the percentage relative variation at the 95% confidence level was estimated for 1 to 1000 polished sections (Figure 18). On each polished section approximately 1200 points on sulphide were analysed by EDS. Based on these results it was decided to do measurements on ~10 polished sections (12 000 points on each sample), thereby achieving a relative error of ~20 per cent or less for the relative proportions of the major sulphide phases. Under these conditions the total error (relative) associated with the absolute volume per cent of the individual sulphides is approximately 45 per cent.*

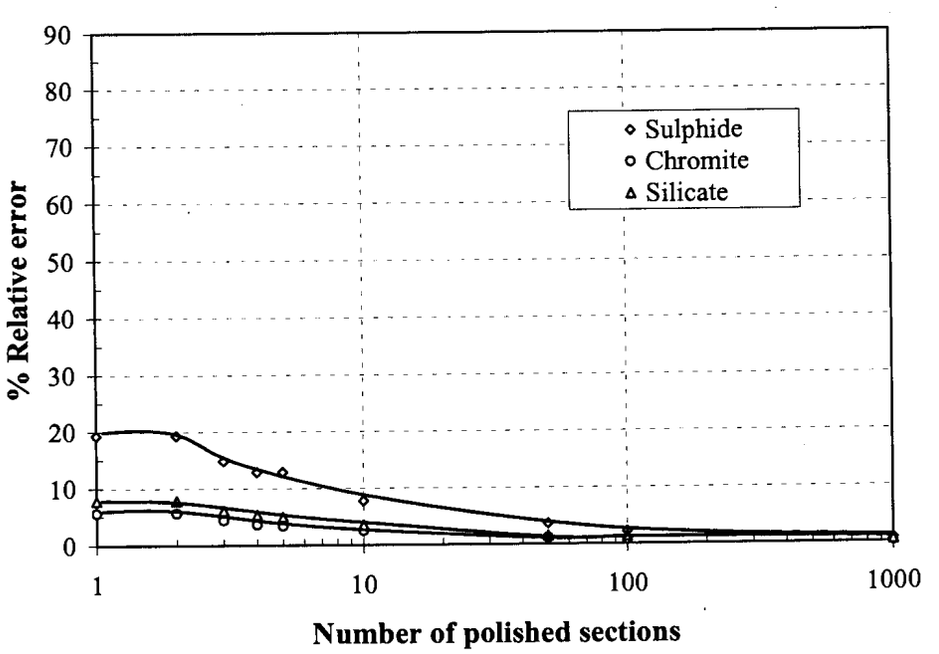

Figure 17 *% Relative error of the modal estimates of base-metal sulphide, chromite and silicate in milled UG2.*

---

* For example: Total BMS = 0.10± 0.04 volume % (~40% relative error) and pentlandite = 49± 10% of total BMS (~20% relative error). Total error^2=Error1^2+Error2^2=45% ∴ Absolute value of pentlandite =0.05±0.02 volume %.

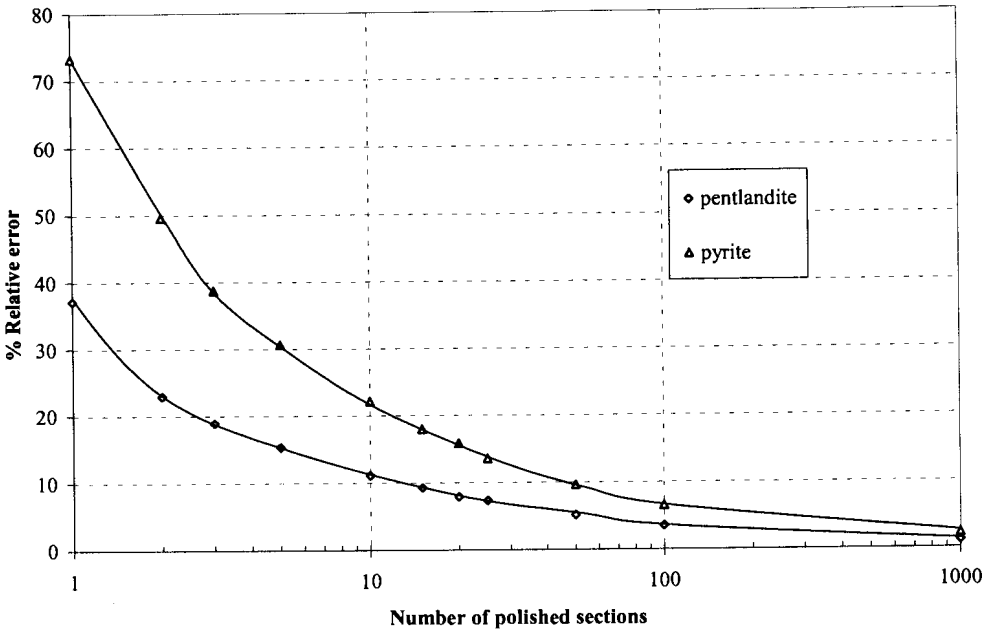

Figure 18 *Effect of the number of polished sections measured on the % relative error in measured pentlandite (at 49 % of total sulphide) and pyrite (at 8% of total sulphide) at the 95% confidence level. Approximately 1200 points were counted on sulphide for each polished section.*

Silicate modal analysis

Image analysis combined with EDS point analysis was also used for silicate modal analysis. Due to the qualitative nature of the EDS analysis and the short analysis time (1s/point) employed, phases with similar chemical compositions, such as talc and bronzite could not be reliably distinguished during the automated analysis. The following 'phases' were recognised: Ca-Al-silicate (predominantly plagioclase, but also includes prehnite, pumpellyite and epidote), Mg-Fe-silicate (predominantly orthopyroxene, minor talc, and rarely serpentine and olivine), phlogopite, clinopyroxene, quartz, chlorite, amphibole, albite, and K-Al-silicate (K-feldspar and sericite).

4.6.4 Chromite and silicate grain-size distributions

Crushed samples

Statistical analysis of measurements on fifteen polished sections of sample A1 indicates that measurements on five polished sections per sample (±15000 chromite

grains) is sufficient to provide a median chromite grain-size value within a 2% error range at the 95% confidence level (Table 1, Appendix C).

Milled feed and flotation products

Due to the homogenising effect of milling, measurements on a much lower number of grains are needed to provide a median chromite grain-size value at the same level of confidence in milled feed and flotation product samples. Data collected along twelve traverses of a polished section of milled feed, showed that measurements on ±5000 chromite grains (two traverses) provide a median chromite grain-size value within a 2% error range at the 95% confidence level (Table 2, Appendix C). The same statistics hold for silicate particle-size measurements.

4.6.5 Base-metal sulphide grain-size distribution and mode of occurrence

Grey level overlaps between different base-metal sulphides and, in the case of milled feed and flotation product samples, between sulphides and stainless steel, coupled with fine grain sizes and low concentration levels, culminated in impractically long analysis times.† For this reason the grain-size distribution and mode of occurrence of individual base-metal sulphide phases were not measured.

Grain-size distribution

Based on statistical analysis of measurements on 30 polished sections of crushed sample A1, it was determined that measurements on more than 100 polished sections are required to provide a median sulphide grain-size value within a <10 per cent error range at the 95% confidence level. For practical reasons, it was decided to perform measurements on between 5 and 10 polished sections per sample.

---

† A relatively coarse grid could be used to determine the relative proportions of the individual base-metal sulphides. To obtain textural information (grain size and mode of occurrence) on individual base-metal sulphides, a very fine grid would have to be used, culminating in long analysis times. Therefore, although the relative amounts of the individual base-metal sulphides could be determined, no textural information could be obtained.

Mode of occurrence and liberation

Base-metal sulphide-bearing particles were classified as liberated if more than 80 per cent of the total area of the particle consisted of sulphide.

4.6.6 PGE mineral characterisation

Problems associated with the characterisation of the UG2 PGE mineral assemblage

Mineral identification

The PGE minerals in the UG2 chromitite generally occur as very small grains (typically <5 μm diameter) making locating and identifying these grains very difficult. Hiemstra (1988a) reported that tests conducted at Mintek showed that many of the smaller PGE mineral grains were not recognised during a manual search using an optical microscope, even by experienced workers.

Although this task becomes easier with the aid of an SEM equipped with EDS, the process mineralogist is often confronted with a finely milled sample, frequently containing significant concentrations of contaminants with high BSE intensities such as brass and stainless steel. A polished section of a flotation tailings sample, for example, may contain several hundred or thousand particles of stainless steel, and less than ten PGE mineral grains. Recognising PGE mineral grains under these conditions is a problem, especially when they have been liberated from the mineral matrix.

Low concentration levels

A number of workers have pointed out the problems in collecting data on a statistically adequate number of grains of trace amounts of minerals in general (Jones & Gavrilovic, 1968; Oosthuyzen, 1985; Cook, 1990), and PGE minerals in particular (Hiemstra, 1988a; Lea, 1996). The low PGE concentration levels in UG2 flotation feed and tailings samples means that a large number of polished sections have to be examined to obtain statistically reliable data.

The question of just how many PGE mineral grains represent a statistically adequate sample will be addressed in a later paragraph. For the moment, suffice it to say that manual collection of data is a tedious, time-consuming and subjective exercise.

Introduction to automated trace-mineral searches

Jones and Gavrolic (1968) made the first documented automated electron microscope-based search for trace amounts of mineral phases. Although it was an excruciatingly slow procedure, it did demonstrate the value of this type of investigation.

Since then, researchers have used integrated systems consisting of various combinations of image analysers and electron microscopes, equipped with energy- or wavelength-dispersive X-ray analysers, to automatically search for trace amounts of Au and/or PGEs:

- Leica Cambridge morphochemical analysis system at Mintek in South Africa (Penberthy & Oosthuyzen, 1992)
- MP-SEM-IPS system at Canmet in Canada (Petruk, 1988a; Walker *et al.*, 1989, Lastra *et al.*, 1999)
- ALF at CSIRO in Australia (Harrowfield *et al.*, 1988; McDonald *et al.*, 1991a; 1991b; McDonald & Sparrow, 1992)
- QEMScan system at CSIRO (Gottlieb *et al.*, 1993)

There are major differences between these systems. The purpose of this investigation is not to discuss the merits of the different systems. Considering the fast pace at which technology is improving, this is in any case a difficult, if not impossible task.

Development of the search routine

During the course of this investigation, it was realised that fully automated characterisation of the PGE minerals of UG2 ore and mineral processing products is an unrealistic goal:

- Firstly, the success of fully automated particle classification depends on particles not touching. This can be achieved by screening each sample into a number of size fractions and adding a filler such as graphite to physically separate sample particles (Miller *et al.*, 1982; Jackson *et al.*, 1984). The reasons for not following this approach, is discussed in section 4.5.2.

  Although image-analysis algorithms to separate touching grains are available, they do not work well on unsized samples or on very fine-grained size fractions. Since

a large proportion of the PGE minerals in the UG2 flotation feed and products are liberated and fine-grained, this is not a viable option for these samples.

One possible approach is to simply assume that all grains in the very fine size fraction (<10 µm) are liberated. Data collected during this investigation however showed that this is not a correct assumption - more than 80 per cent of the PGE mineral-bearing particles in the feed sample at 80% <75µm are finer than 10 µm. Of these fine particles, 27 per cent consists of locked PGE minerals. In addition, information on chemical composition, albeit qualitative, and textural features will be lost by this approach.

- Secondly, the small grain-size and mode of occurrence of PGE minerals in the UG2 ore simply does not lend itself to automated characterisation by X-ray analysis - most of the PGE minerals are smaller than 5µm diameter, and a significant proportion (7 to 8 per cent) occurs as composite PGE mineral grains (e.g. laurite + cooperite). Under these conditions, the short EDS acquisition times typically used during this type of analysis, combined with the poor spatial resolution for X-rays, (2 to 8 µm compared with 0.05 to 0.1 µm for the BSE signal (Gu, 1998)), and the overlap between the X-ray peaks of the different PGEs on an EDS spectrum, do not provide accurate enough data for automated measurement and classification.

For the purpose of this investigation, the samples were therefore analysed unsized and undiluted. A two-stage approach was adopted: The first stage consists of a fully automated, unsupervised routine that simply searches for PGE minerals and records the co-ordinates, without attempting to classify the grains in terms of mode of occurrence or chemical composition (Figure 19). Potential PGE minerals are identified by the high BSE intensity of these phases. A sample containing a 0.5µm grain of laurite, together with cooperite, chalcopyrite and stainless steel is used as a standard to set the grey-level window. If a field contains a potential PGE mineral grain, a digital image transfer is done followed by EDS analysis at the centroid of the grain (1s/grain). The purpose of the EDS analysis is to exclude other particles with high BSE intensity such as galena, brass, and stainless steel. Co-ordinates of PGE mineral grains are stored in a file. During such a run several polished sections are searched, usually overnight. As a control on beam stability, the grey levels and areas

of the phases in the standard field were measured before and after scanning of each polished section. If the measured values were different to those measured during set-up of the run, the results were rejected and the run repeated at a later stage.

The second stage of the analysis consists of a menu-driven interactive routine (Figure 20) during which the stored co-ordinates of each PGE mineral grain is recalled automatically, followed by semi-automated determination of the qualitative chemical composition and area of each PGE mineral grain and associated phases. This information is recorded and stored for off-line statistical evaluation.

Statistical considerations

Apart from any operational errors, the results of such a search may not accurately reflect the true nature of the mineralogy of the PGE minerals for two reasons:

Spatial resolution

If too low a magnification is used, then grains at the lower end of the size range will not be detected during the search. At 200x magnification, 1 pixel is equivalent to 0.79 µm. At this magnification ±1000 fields are scanned on each polished section, covering an area of ~1.8 cm^2. To effect even a small improvement in resolution beyond this value requires that a significantly larger number of fields have to be searched to cover the area of a polished section (Figure 21). The average search time under these conditions are 3 hours per polished section, but varies between 1.5 and 7 hours depending on the nature of the sample.

Nugget effect

Enough polished sections have to be searched to collect data on a statistically representative sample of the PGE minerals in any sample. For example, a search of 146 polished sections of crushed UG2 chromitite yielded data on 4000 PGE mineral grains. Although less than 2 per cent (76 grains) of these grains are coarser than 10 µm, they represent almost 30 per cent of the total area of PGE mineral found (Figure

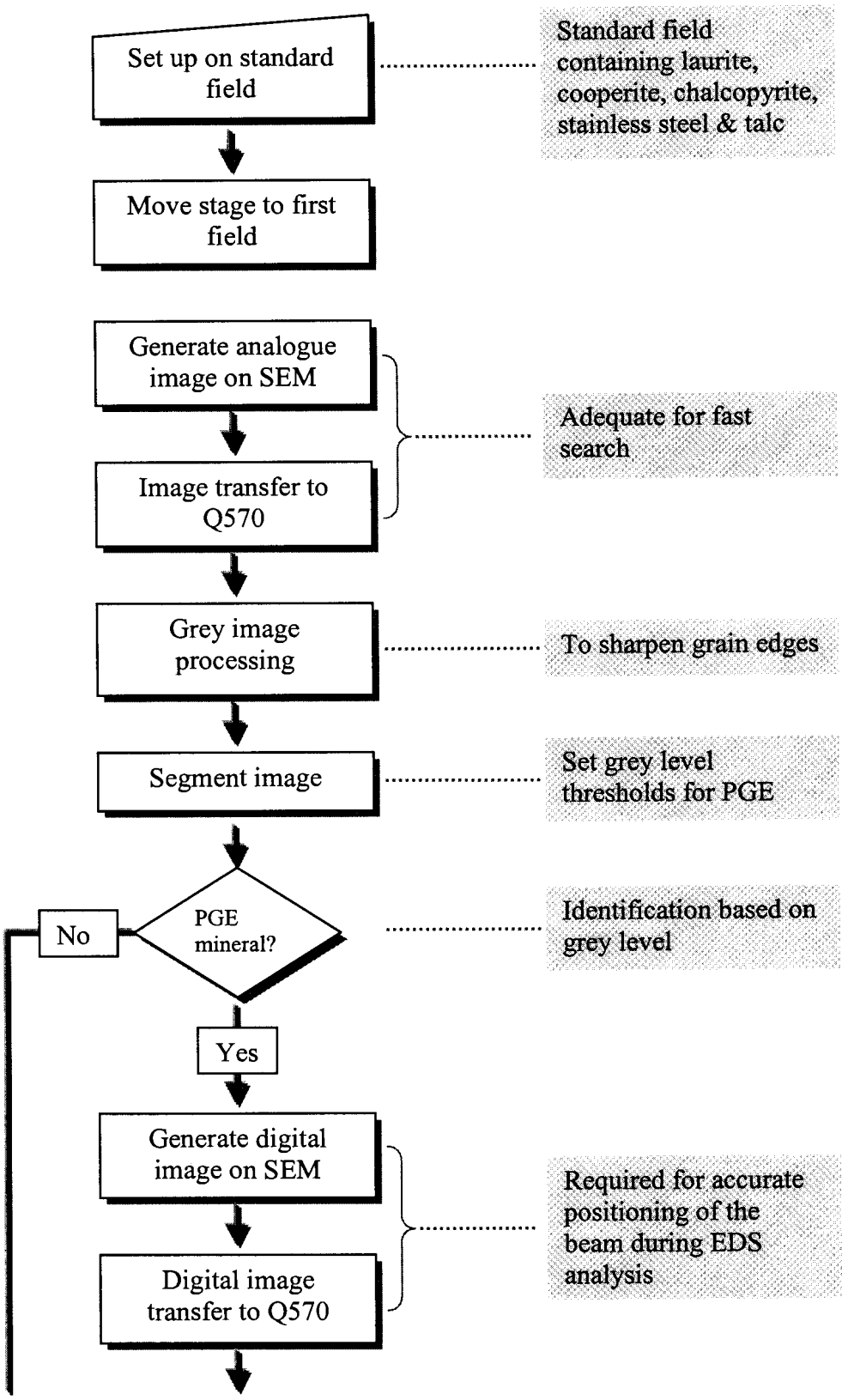

Figure 19 *Flow diagram for automated PGE mineral search.*

p.t.o.

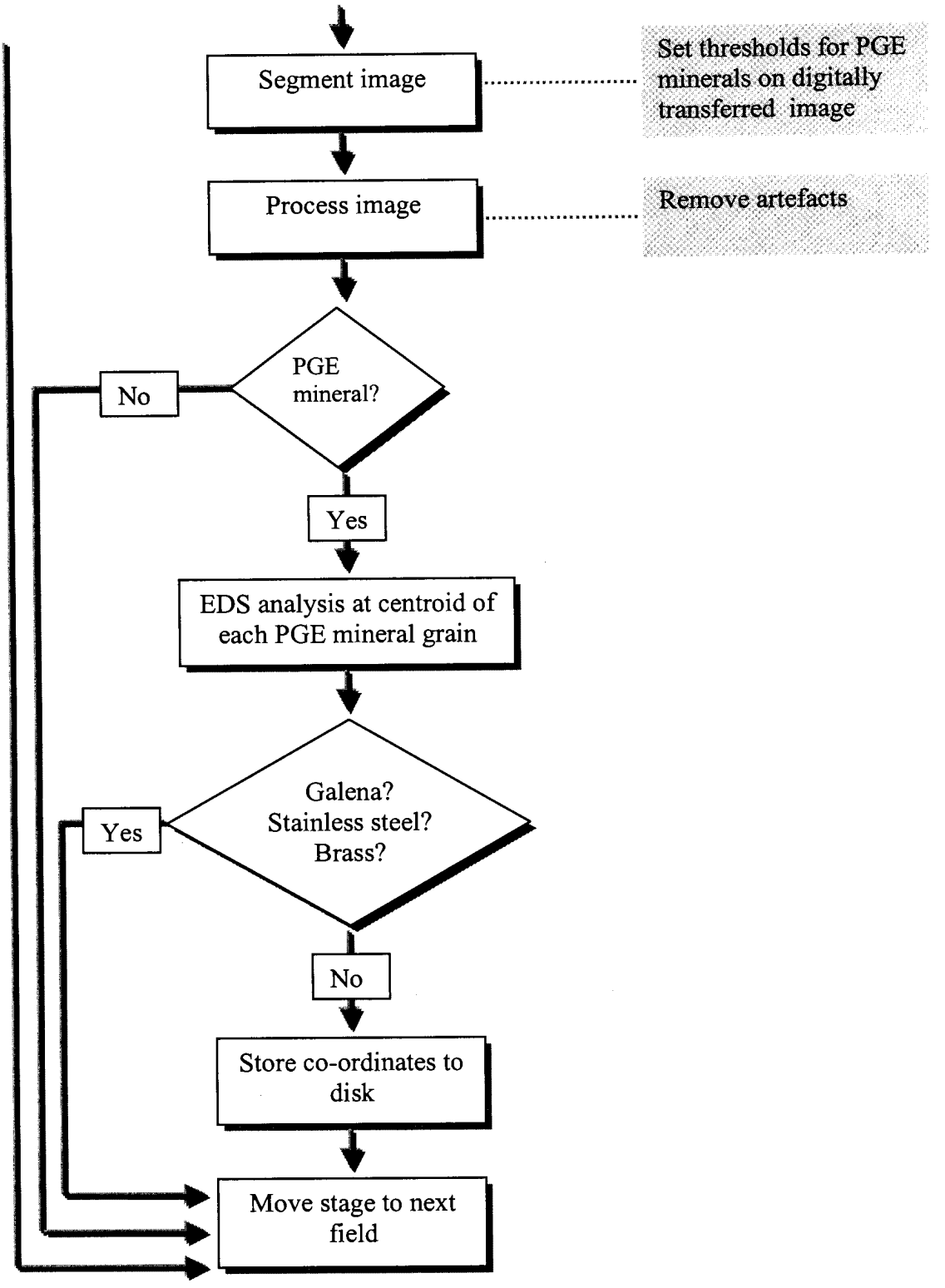

Figure 19 continued *Flow diagram for automated PGE mineral search.*

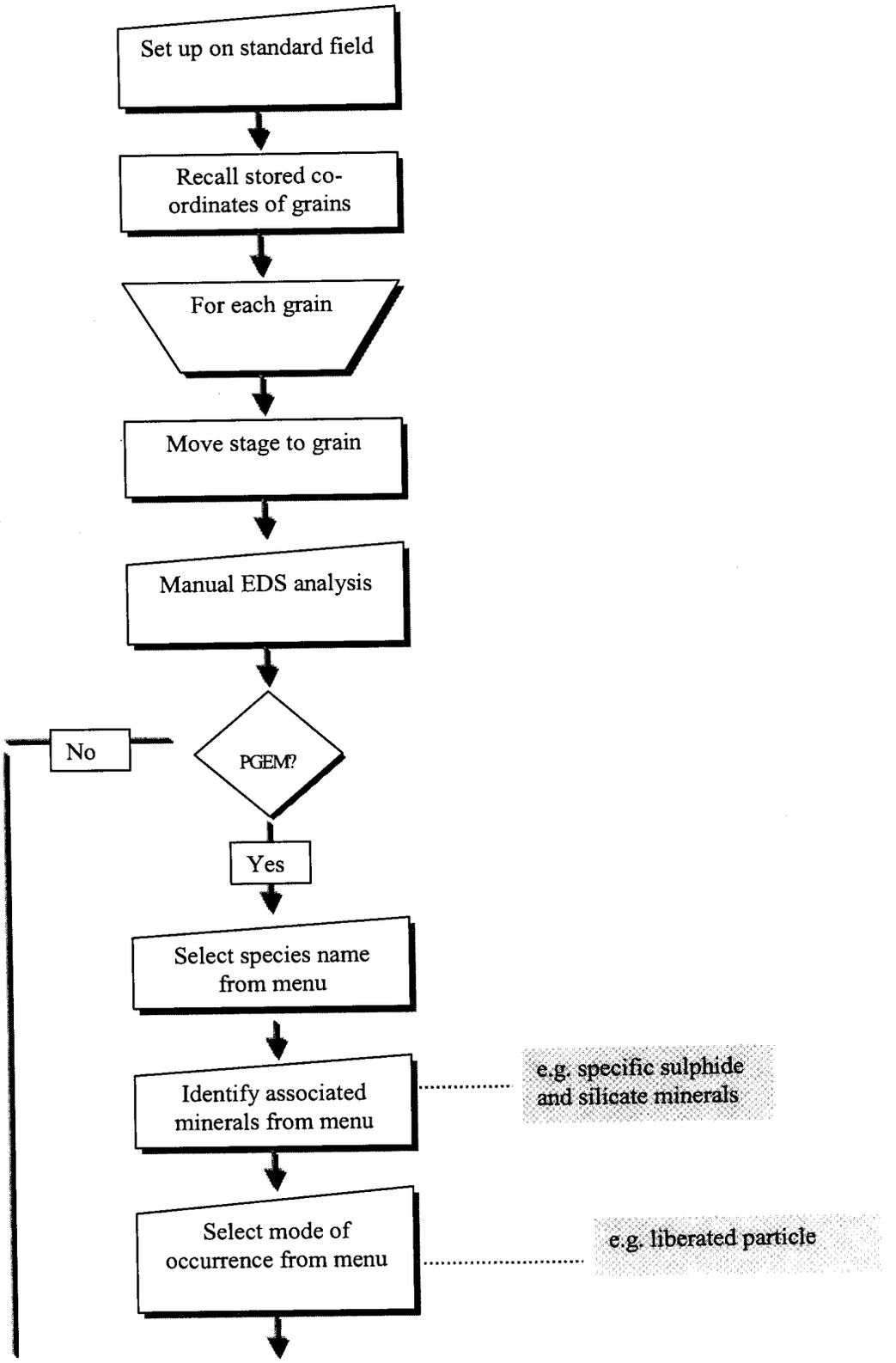

Figure 20 *Flow diagram for semi-automated measurement and classification of PGE minerals.*

p.t.o.

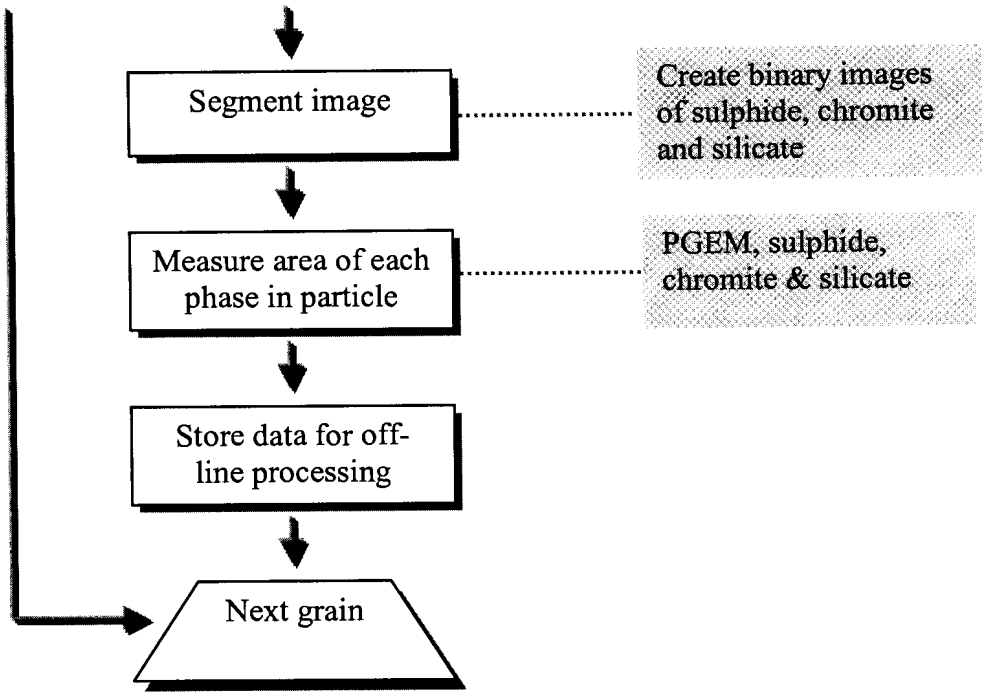

Figure 20 continued *Flow diagram for semi-automated measurement and classification of PGE minerals.*

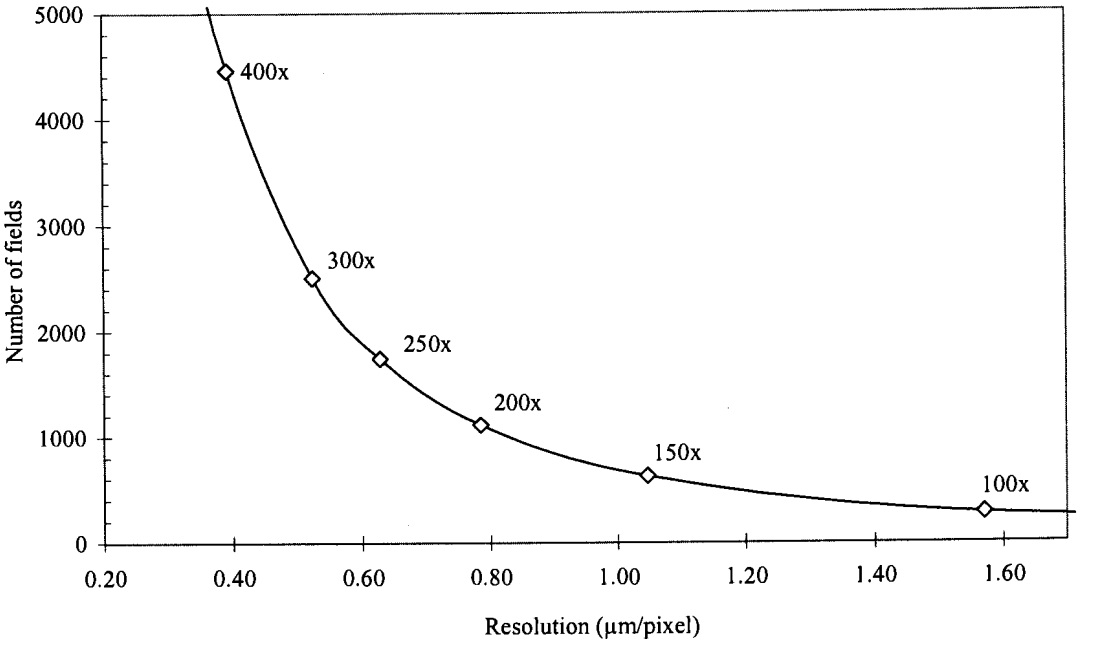

Figure 21 *The relationship between spatial resolution (µm per pixel) on a BSE image at different magnifications, and the number of fields of view required to cover the area of a polished section.*

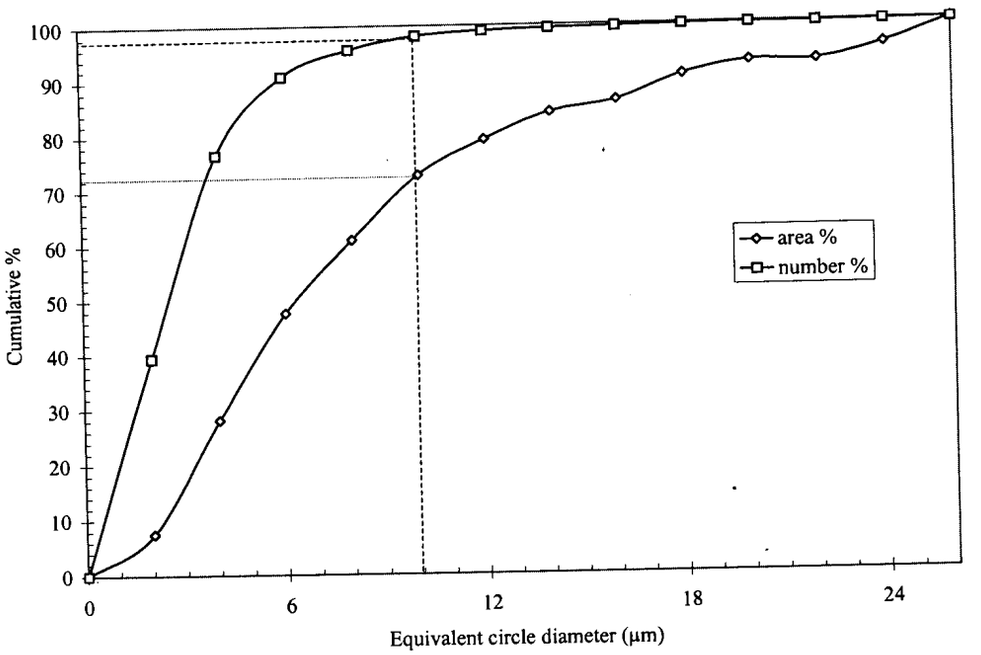

Figure 22 *Grain-size distribution of 4000 PGE mineral grains found in crushed UG2 chromitite.*

22). In addition, although one can expect to find an average of one >10 µm PGE mineral grain in every two polished sections, statistically there is only a 37 per cent probability that such a grain will be found in any specific two polished sections (see also Jones & Gavrolic, 1968).

It should be kept in mind that one grain with a diameter of 10 µm has an area equivalent to that of one hundred 1µm grains. This so-called nugget effect (Oosthuyzen, 1985) can lead to the overestimation or underestimation of the amount of PGE mineral if an insufficient number of polished sections are searched. This effect is demonstrated by data collected during analysis of sample A1 (Figure 23).

A new value for Σ(Pt+Pd+Rh) was calculated from the modal composition following the measurement of each of eighty polished sections.[+] The percentage relative error at

---

[+] Average mineral compositions obtained by electron-microprobe analyses were used as far as possible (Appendix G). For phases for which electron-microprobe analyses

the 90% confidence limit in the calculated value of Σ(Pt+Pd+Rh) associated with different numbers of PGE mineral grains was calculated using resampling statitistics (Figure 24). To obtain an error of less than 10 per cent, data on approximately 3000 grains are required. A practically attainable number of grains is ~200 (except in the flotation tailings), which yields an error of 30 to 40 per cent.

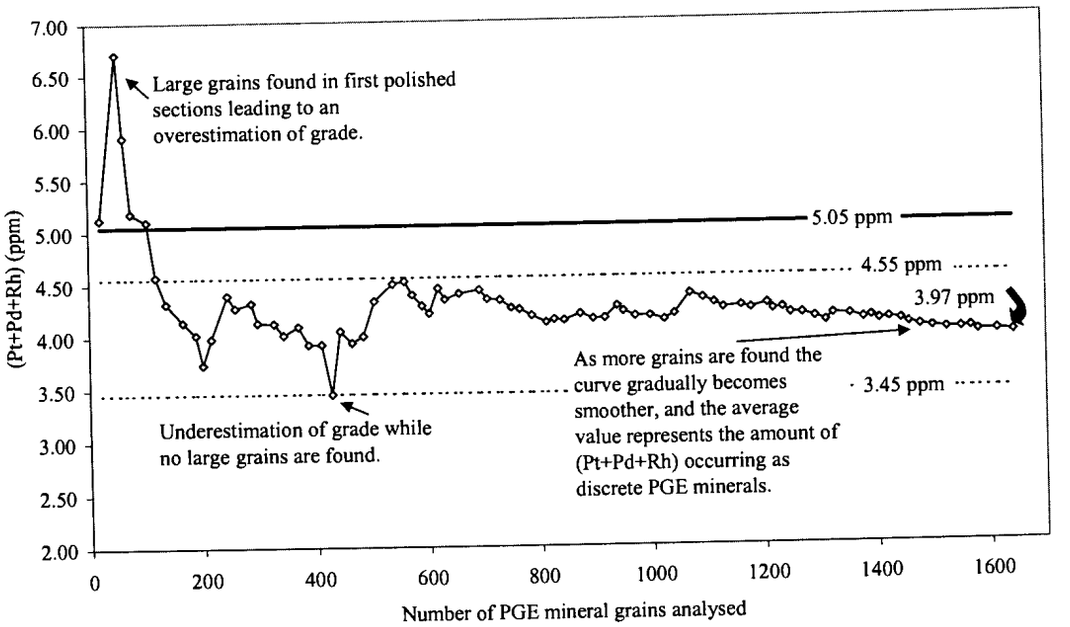

Figure 23 *Variation in Σ(Pt+Pd+Rh) calculated from the mineralogical composition depending on the number of PGE mineral grains recorded. The two dashed horizontals at 3.45 ppm and 4.55 ppm represent the 90% confidence interval for 1642 grains found in 80 polished sections. The chemical assay value of 5.05 ppm is indicated by the solid horizontal.*

PGE mineral modal distribution

During the course of this study more than 25 chemically distinct PGE mineral phases were observed. PGE mineral phases were classified according to the presence of

---

were not available, ideal mineral compositions were assumed (Appendix B). Mineral densities used are listed in Appendix B. Pycnometer measurements indicated a density of 3.87 for sample A1. A density value of 3.85 was calculated from modal analysis data.

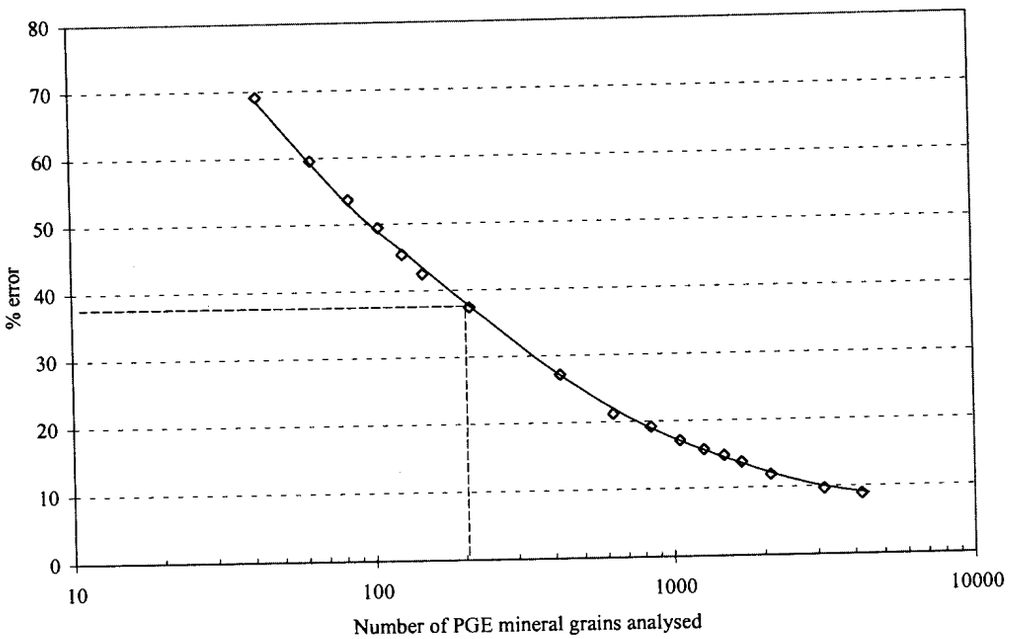

Figure 24 *% Error in the calculated assay value at the 90% confidence limit associated with different numbers of PGE mineral grains.*

major elements identified using qualitative EDS analysis. Due to resolution limitations, the presence of nickel, copper, cobalt and iron can not always be established during analysis of small PGE mineral grains included in base-metal sulphides. For this reason, these elements are not specifically mentioned in the text unless they constitute a substantial component of the PGE mineral concerned e.g. Pt-Fe alloy. Quantitative electron-microprobe analysis of selected grains was used to confirm the identities of the most commonly occurring phases. For practical purposes these phases can be grouped together in the following eight categories:

- Pt-Pd-Ni-sulphide (braggite and less commonly vysotskite)
- Pt-S (probably mostly cooperite)
- Pt-Rh-Cu-Ni-S (probably mostly nickeloan malanite, usually cobalt-bearing)
- Ru-Os-Ir-S (laurite-erlichmanite), as well as rare grains of metallic Ir-Ru-Os.
- PGE-Bi-Te (various tellurides, bismuthinides and bismuthtellurides of platinum and palladium)
- PGE-As±S (includes a variety of sulpharsenides and arsenides such as hollingworthite, irarsite, ruarsite, sperrylite and majakite)

- Pt-Fe (alloys of platinum and iron, often contain palladium and rhodium, sometimes copper)
- Other non-sulphide (a host of minerals, usually palladium-bearing, consisting of various compounds of PGEs with Hg, Pb, Ge, Sb, As, Bi, Te and Sn).

Using the data on 665 and 619 PGE mineral grains for the crushed and milled feed samples of sample A1 respectively, the precision was calculated for a random sample of 200 grains (Table 4.13). The higher degree of precision in the milled sample is a reflection of the homogenising effect of milling.

Table 4.13 *Modal proportions of PGE minerals in sample A1 and the error (absolute) at the 90% confidence limit associated with a sample of 200 grains. Error calculated using resampling statistics (Simon & Bruce, 1991).*

PGE Phase	*Modal %*	*<2 mm ±%*	*80% <75µm ±%*
Pt-Pd-Ni-S	34	17	12
Pt-S	20	15	9
Pt-Rh-Cu-Ni-S	18	12	10
Ru-Os-Ir-S	18	10	7
PGE-Bi-Te	2	3	3
PGE-As±S	3	5	3
Pt-Fe	2	2	1
Other non-sulphide	2	3	3

PGE mineral mode of occurrence

All PGE mineral grains observed in crushed ore were classified according to their textural setting into one of the following categories (Table 4.14):

- Liberated PGE mineral grains, i.e. grains that were freed from the rock matrix during crushing. Most of these grains were probably located at grain boundaries prior to size reduction.
- Locked in base-metal sulphide, refers to PGE mineral grains enclosed in base-metal sulphide composite grains, including PGE mineral grains at sulphide-sulphide grain boundaries.

- Locked in oxide, refers to PGE mineral grains enclosed in oxide minerals, usually chromite, rarely rutile or magnetite.
- Locked in silicate, includes PGE mineral grains occurring both as inclusions in silicate and at silicate-silicate grain boundaries.
- PGE mineral grains occurring at the grain boundaries of base-metal sulphide with silicate and/or chromite.
- PGE mineral grains occurring at the grain edges of chromite and/or silicate, i.e. at the grain boundary of mineral and mounting resin.

Table 4.14 *Mode of occurrence of PGE minerals in sample A1 crushed to <2mm and the precision at the 90% confidence limit associated with a sample of 200 grains. Absolute error calculated using resampling statistics (Simon & Bruce, 1991).*

Mode of occurrence	*Area %*	*±%*
Liberated PGEM	7	9
PGEM locked in BMS	26	14
PGEM locked in oxide	2	1
PGEM locked in silicate	2	2
PGE at GB BMS/Gangue	57	16
PGE at gangue grain edge	6	7

In the case of milled samples an even simpler classification was adopted (Table 4.15).

Table 4.15 *Mode of occurrence of PGE minerals in sample A1 milled to 80% <75µm and the precision at the 90% confidence limit associated with a sample of 200 grains. Absolute error calculated using resampling statistics (Simon & Bruce, 1991).*

Mode of occurrence	*%*	*±%*
Liberated PGEM	57	12
PGEM + liberated BMS	29	11
PGEM ± (BMS)+ Gangue	14	6

In addition, a combined liberation index was calculated for all PGE mineral-bearing grains (Figure 25 and Table 4.16): *Combined liberation index = area of floatable mineral in particle/total area of particle* where *floatable mineral = BMS and PGEM.* This calculation yields a value between 0 and 1, with 1 indicating a particle consisting of a liberated PGE mineral grain, or, a PGE mineral attached to, or locked in a liberated base-metal sulphide grain. A particle consisting of a large silicate grain with a small PGE mineral inclusion will be characterised by a combined liberation index approaching 0. †

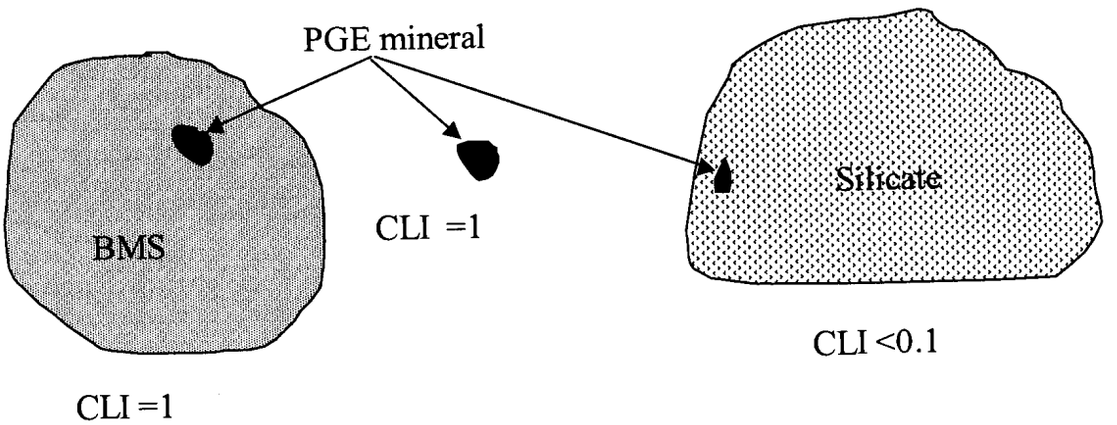

Figure 25 *Graphical representation of three PGE mineral-bearing particles illustrating the combined liberation index (CLI) principle.*

† A liberation index based on area measurements does not always give a true reflection of floatability, which depends on exposed surface area. For instance, a large PGE mineral grain rimmed by silicate may have a high CLI, but will not be recoverable by flotation. However, in the case of small grains, perimeter measurements necessary for the calculation of exposed surface area are inaccurate, hence the decision to base the liberation index on area measurements.

Table 4.16 *Combined liberation index of PGE minerals in sample A1 at 80% <75µm, and precision at the 90% confidence limit associated with a sample of 200 grains. Absolute error calculated using resampling statistics (Simon & Bruce, 1991).*

Combined liberation index	*Area %*	*± %*	*Cumulative area %*
0.0-0.2	16	9	16
0.2-0.4	1	1	17
0.4-0.6	0	1	17
0.6-0.8	0	0	17
0.8-1.0	83	9	100

PGE mineral grain-size distribution

A PGE mineral grain-size distribution was also calculated for each sample. From the grain-size distribution a median value was calculated both in terms of number of grains and area. The errors associated with the median values calculated from a sample of 200 grains for sample A1 at <2mm and at 80%<75µm are given in Table 4.17. These values demonstrate that, for a sample of 200 grains, the median grain size based on per cent number of grains is statistically more reliable, than the median grain size based on area per cent. Thus, although the median grain size based on per cent number of grains is not a very good reflection of the true grain size, it does allow for comparisons between samples.

Table 4.17 *Median grain diameter of PGE minerals in sample A1 at <2mm and 80% <75µm, and precision at the 90% confidence limit associated with a sample of 200 grains. Error calculated using resampling statistics (Simon & Bruce, 1991).*

	Median (µm)	*± (µm)*
<2 mm by area	7.2	3.7
<2 mm by number	2.2	0.1
80%<75 µm by area	3.9	1.5
80%<75 µm by number	2.2	0.2